ARCHIVIO ISTITUZIONALE
DELLA RICERCA

Alma Mater Studiorum Università di Bologna
Archivio istituzionale della ricerca

Assessment of the accuracy of scaling methods for radiance simulations at far and mid infrared wavelengths

This is the final peer-reviewed author's accepted manuscript (postprint) of the following publication:

Published Version:
Martinazzo, M., Magurno, D., Cossich, W., Serio, C., Masiello, G., Maestri, T. (2021). Assessment of the accuracy of scaling methods for radiance simulations at far and mid infrared wavelengths. JOURNAL OF QUANTITATIVE SPECTROSCOPY & RADIATIVE TRANSFER, 271, 1-20 [10.1016/j.jqsrt.2021.107739].

Availability:
This version is available at: https://hdl.handle.net/11585/822909 since: 2021-06-19

Published:

DOI: http://doi.org/10.1016/j.jqsrt.2021.107739

Terms of use:

Some rights reserved. The terms and conditions for the reuse of this version of the manuscript are specified in the publishing policy. For all terms of use and more information see the publisher's website.

This item was downloaded from IRIS Università di Bologna (https://cris.unibo.it/).
When citing, please refer to the published version.

(Article begins on next page)

10 January 2025

This is the final peer-reviewed accepted manuscript of:

Michele Martinazzo, Davide Magurno, William Cossich, Carmine Serio, Guido Masiello, Tiziano Maestri, *Assessment of the accuracy of scaling methods for radiance simulations at far and mid infrared wavelengths*, Journal of Quantitative Spectroscopy and Radiative Transfer, Volume 271, 2021, 107739.

The final published version is available online at: https://doi.org/10.1016/j.jqsrt.2021.107739

Terms of use:

Some rights reserved. The terms and conditions for the reuse of this version of the manuscript are specified in the publishing policy. For all terms of use and more information see the publisher's website.

This item was downloaded from IRIS Università di Bologna (https://cris.unibo.it/)

When citing, please refer to the published version.

Assessment of the accuracy of scaling methods for radiance simulations at far and mid infrared wavelengths

Michele Martinazzo[a], Davide Magurno[a], William Cossich[a], Carmine Serio[b], Guido Masiello[b], Tiziano Maestri[a,*]

[a] *Department of Physics and Astronomy, University of Bologna, via Irnerio 46, 40126, Bologna, Italy*
[b] *School of Engineering, University of Basilicata, Viale dell'Ateneo Lucano 10, 85100, Potenza, Italy*

Abstract

Top of the atmosphere synthetic spectral radiances are computed for widespread atmospheric conditions by alternatively using the discrete ordinate algorithm solution or approximate methodologies where the scattering effects are simulated by appropriate scaling of the absorption properties of the diffusive layers. The residuals between the full scattering solution and the scaling methods are evaluated at far- and mid- infrared wavelengths and compared with the goal noise of the FORUM (Far-infrared Outgoing Radiation Understanding and Monitoring) satellite sensor, that will be the next European Space Agency (ESA) 9^{th} Earth Explorer, capable of spectrally resolved measurements in the 100–1600 cm^{-1} band. The results define the limit of validity of the fast methodologies considered: the Chou approximation, that is provided as an improved version, and a simple scaling based on the similarity principle. In particular, it is shown that in case of water clouds the scaling methodologies are sufficiently accurate in the mid infrared, except when very small effective radii are accounted for, independently of the cloud optical depths. The same holds in the far infrared for low level water clouds and for humid regions, while not negligible inaccuracies are observed in an increasingly dry atmosphere above the cloud and for small

*Corresponding author
Email address: tiziano.maestri@unibo.it (Tiziano Maestri)

effective radii. Ice clouds are accurately simulated by scaling methods at mid infrared wavelengths in all conditions and for very optically thin clouds at far infrared. Nevertheless, the computational errors become larger than the FORUM noise for optical depths of the order of unity at far infrared. Examples of desert dust and volcanic aerosol are also analysed, showing that the approximate solutions could drive to significant errors also at mid infrared wavelengths.
Keywords: cloud, fast code, FORUM, infrared, radiative transfer, scattering

1. Introduction

With the era of satellite missions for environmental and meteorological applications, radiative transfer in the Earth's atmosphere has become a topic which is at the forefront of all physically-based remote sensing applications. Today, the basic principles and equations can be found in many textbooks and tutorials, e.g. [1, 2, 3]. Nevertheless, specific applications still need research work because of the inter-relationship between optical properties of the matter and absorption, emission and scattering processes.

In the framework of satellite applications, early use of radiative transfer calculations was limited to clear sky with a simplistic one-layer opaque cloud (emissivity equal to 1), e.g. [4, 5]. However, the importance and significance of clouds' impact on weather and climate has made researchers develop suitable schemes to solve the fundamental equations in a cloudy atmosphere and take into account radiative effects that are computationally expensive, such as multiple scattering. In effect, one result soon achieved with satellite observations is that the Earth globe is, on average, covered by clouds by more than 80% [1]. It is now well recognized (e.g. [6]) that cloud identification and properties retrieval is fundamental for the definition of the radiative balance at the surface and at the top of the atmosphere, and that assessing the impact of clouds on the global circulation represents a significant task in improving climate models.

The present study focuses on the accuracy of simple, scaling, *analytical* approximations to solve the radiative transfer equation in the infrared in the pres-

ence of clouds and aerosols, when the simplifying hypothesis of no scattering atmosphere, which is used in clear sky conditions, is no more valid. In fact, analytical approximations, such as that introduced by [7], allow us to extend clear sky hyper-fast radiative transfer models to scattering conditions. The gain in term of computational time is impressive since these approximate radiative transfer algorithms can provide high spectral radiance field simulations over the full infrared spectrum in less than a second, compared to times of the order of tens or hundreds of minutes (depending on cloud properties) employed by full scattering radiative transfer codes.

Moreover, the present study is motivated by the need to check the accuracy of suitable fast multiple-scattering schemes for the FORUM (Far-infrared Outgoing Radiation Understanding and Monitoring) sensor, a Fourier Transform spectrometer to be launched in 2026 in the context of the ESA 9^{th} Earth Explorer. FORUM will be capable of measuring spectrally resolved radiances in the 100–1600 cm^{-1} band (e.g. see [8]).

As far as the infrared spectral range is concerned, suitable *numerical* methods (e.g. doubling-adding and discrete ordinate methods) for the radiative transfer equation do exist and have been primarily used to retrieve optical properties of aerosols and clouds (e.g. [9, 10] and references therein). In this respect, we note that one of the most popular numerical schemes for multiple scattering, that is DISORT (Discrete Ordinate Radiative Transfer [11]), has been coupled to LBLRTM (Line-by-Line Radiative Transfer Model [12]) to yield LBLDIS [13]. We have also to note here the development of schemes specialized for few channels aiming at retrieving properties of cirrus clouds (e.g. [14]).

However, radiative transfer calculations with numerical, multiple scattering schemes have a huge computational burden and are not amenable to be included in the fast forward model developed for data assimilation [15] in numerical weather prediction centers or for the purpose of fast operational retrievals for geophysical parameters and atmospheric composition (e.g. [16, 17]). In the framework of fast and hyper-fast models, analytical, approximate methods are desirable, because numerical solutions are too computationally expensive.

A step forward in this direction was made by [7], who developed a scheme (hereinafter – the Chou scaling approximation or CA) where the scattering effect by clouds and aerosols is parameterized by scaling the optical depth by a factor which includes hemispheric backscattering in the emission of a layer and in the transmission between levels. The multiple scattering parameterization is based on the hypothesis that the longwave radiation field is isotropic.

CA was introduced and intended for flux computations [7]. However, it has been proved that CA is also useful for radiance calculations (e.g., [18]). CA scaling approximation has the advantage that the used form of the radiative transfer equation in cloudy skies is identical to the general form used for a clear atmosphere, therefore, the computational efficiency of a given radiative transfer model (RTM) is not degraded. Since CA handles scattering as a scaling of the absorption OD, the vertical profile concentration of aerosol, liquid water, and ice particles can be treated as gases in the mid and far infrared.

CA was first implemented for spectral radiance calculations in [18], and soon after used in 1-D variational data assimilation of high spectral resolution, infrared radiance from satellite [19]. Today, it is routinely adopted for radiance computation in fast RTMs (e.g. [20, 21, 17, 22]). An in-depth inter-comparison of diverse, fast forward models for cloudy atmosphere, not only using CA, has been recently performed by [23]. The results show that the main differences among the codes arise from the way they deal with geometrical and geophysical parameters such as the cloud fraction and the database used for optical properties of ice and liquid water, rather than on radiative transfer methodology and approximations.

Until now, the accuracy of CA has been assessed mainly in the thermal infrared ($\approx$ 645 to 3000 cm^{-1}), which is the range of modern hyper-spectral infrared sensors, whereas an assessment of the accuracy of fast analytical approximations for the far infrared (FIR, $\approx$ 50 to 700 cm^{-1}) spectral region is still incomplete. Yet, the FIR (that is the focus of the FORUM mission) plays an essential role in processes governing the natural greenhouse effect of the Earth (e.g., [24]), including cirrus clouds. Until now, the analysis concerning this

spectral region have been mostly limited to clear sky for observations of the water vapour rotational band and studies concerning the assessment of the H_2O continuum absorption (e.g. [25, 26, 27, 28, 29]). However, the promotion and planning of satellite missions dedicated to the FIR spectral region (e.g., [30, 31]) has renewed the research interest in the field of all-sky RTMs. It has also to be stressed that the FIR spectral region is expected to play a relevant role for the detection and analysis, e.g., of cirrus clouds [32, 33]. Thus, understanding the impact on FIR radiances of multiple scattering analytical approximations, such as that provided by [7], is an important issue, which we address in this paper.

To begin with, we provide an improved CA approximation and compare it to a scaling form based on the similarity principle [34]. Radiance calculations based on these two simple scaling approaches are compared against efficient numerical computations accomplished out with the LBLDIS model. Results are provided for an extensive data set of state vectors, encompassing liquid water, ice, and aerosols. The analysis covers the whole FORUM range (100–1600 cm^{-1}), so that it will be interesting also for users working in the mid infrared.

The paper is organized as follows. The state vectors for ice, liquid water, and aerosols, and related databases for the optical properties are described in Section 2.1. The various scaling approaches are presented and described in Section 2.2. Section 3.1 is dedicated to an improved calculation of the backscattering function introduced in [7]. Results about radiance calculations, performed with the various scaling approximations, and their comparison to LBLDIS computations are shown in Section 3.3. Finally, conclusions are drawn in Section 4.

2. Data and methods

2.1. Data: atmosphere, clouds, and aerosols characterization

Vertical profiles of pressure, temperature, water vapor and ozone volume mixing ratios are derived from the ERA 5 reanalysis data [35] at four latitudes, representative of equatorial, low-, mid-, and high- latitude scenarios (Table 1). Since the ERA 5 data are limited to a maximum level altitude of about 60 km,

Table 1: Main features of the selected scenarios. Data from the ERA 5 database.

Scene	Latitude (°)	Longitude (°)	Date (YYYY-MM-DD)	Time (UTC)	SST (K)	PWV (mm)
Equator	+5	+3	2018-01-15	12:00	301.3	48.2
Low latitude	+34	+19	2017-07-15	12:00	300.2	17.8
Mid latitude	+50	−20	2019-03-13	12:00	283.8	9.1
High latitude	+74	−5	2019-03-13	12:00	272.6*	2.9

*No sea ice is observed despite the SST is below 0°C (`https://nsidc.org/data/seaice_index`)

the vertical profiles are extended up to 80 km using the climatological database IG2 v5.7 [36]. The IG2 is also used for the specification of the volume mixing ratio profiles of ten minor gases (CO_2, N_2O, CO, CH_4, O_2, NO, SO_2, NO_2, NH_3, and HNO_3). The vertical profile of CO_2 mixing ratio, estimated by IG2 in 2013, is linearly corrected to the selected years concentration level by means of a scaling factor. The vertical profiles of temperature and water vapor mixing ratio, from the ground up to 20 km altitude, are shown in Figure 1 for the four selected latitudes. The geolocations correspond to grid points over the sea. The surface emissivity is derived from the database by [37], and the corresponding sea surface temperature (SST) is taken from the ERA 5 dataset. The SST and the total precipitable water vapor (PWV) reported in Table 1 span over a large range of values accounting from a very cold and dry scenario at high latitude to a warm and wet equatorial condition.

For each of the four scenarios reported in Table 1 and Figure 1, simulations assuming, alternatively, the presence of liquid water or ice clouds or aerosol components are performed. The geometrical, optical and micro-physical properties of the scattering layers are not derived from the ERA 5 dataset but systematically varied over a wide range of values in order to account for a large variety of observational conditions. The cloud and aerosol features used in the radiative transfer computations are briefly described in the following sections.

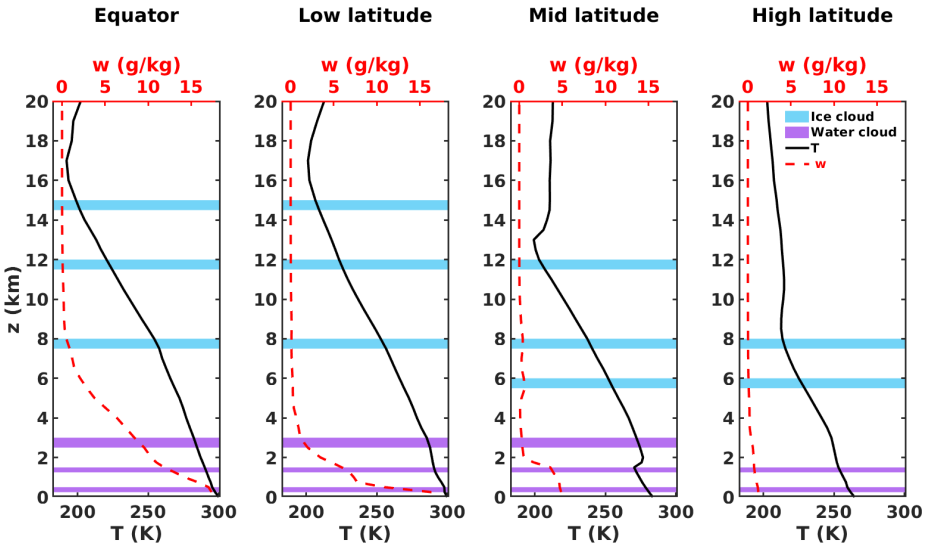

Figure 1: Vertical profiles of temperature (black solid line) and water vapor mixing ratio (red dashed line) for the considered scenarios. Light blue and purple shaded layers show the height position and thickness of the analysed ice clouds and liquid water clouds, respectively.

2.1.1. Liquid water clouds

Liquid water clouds are assumed as composed of a particle size distribution (PSD) of water spheres, whose single scattering single particle radiative properties are generated by using a Mie solution based algorithm, the Scattnlay code [38]. Scattnlay performs calculations of scattering coefficients and efficiency factors as well as scattering phase functions for single, isolated, spherical particles. Water refractive indeces by [39] are ingested for the computations. The single particle properties are then combined to generate single scattering radiative properties for the PSDs over the spectral interval of interest. PSDs of low-level stratiform clouds, as those modelled in this study, are commonly described by a lognormal distribution [40], whose number of particles per unit volume is

$$n(r) = \frac{n_0}{r\sqrt{2\pi}\sigma} e^{-\frac{(\ln(r/r_m))^2}{2\sigma^2}} \tag{1}$$

where r is the particle radius, r_m is the mode radius of the distribution, σ is the scale parameter, and n_0 is a normalization factor that depends on the total

number of particles per volume used in the radiative transfer computations. In this work, the scale parameter is set to σ=0.38, according to the average value derived by [40] from in-situ measurements of low-level stratiform clouds. Assuming σ as a constant, the different PSDs are unequivocally related to their effective radius r_{eff}, defined as the fraction of the third to the second moment of the PSD:

$$r_{eff} = \frac{\int_0^\infty r^3 n(r) dr}{\int_0^\infty r^2 n(r) dr} \tag{2}$$

For a lognormal PSD, the relation between effective and mode radius is derived from Equations 1 and 2 and results to be

$$r_{eff} = r_m e^{\frac{5}{2}\sigma^2} \tag{3}$$

Multiple simulations are performed for different r_{eff}, total optical depth (OD, at 900 cm^{-1}), and cloud top. The ranges of the input parameters, common to every latitudinal scenario, are reported in Table 2. Both for liquid water and ice clouds, six different r_{eff} values are used spanning over the reported ranges. Similarly, ten different OD values are assumed in the simulations. The equation defining the total OD for vertically homogeneous clouds of thickness Δz is

$$OD = N_{tot} \beta(r_{eff}, 900) \Delta z \tag{4}$$

where $\beta(r_{eff}, 900)$ is the extinction coefficient at 900 cm^{-1} of the PSD corresponding to a specific r_{eff}, normalized to a single particle per volume. N_{tot} is the total number of particles in the volume, which is computed internally by the code once the input parameters (OD, r_{eff}, and Δz) are provided. It is assumed that once r_{eff} is selected the corresponding optical properties are unequivocally defined. Liquid cloud layers are shown as purple bands in Figure 1. Ice clouds are in cyan in the same Figure.

Table 2: Values and ranges of the cloud and aerosol parameters used in the selected case studies.

Particle type	PSD type	r_{eff} (µm)	Top Height (km)	Thickness (km)	OD (900 cm^{-1})
Liquid water	lognormal (σ=0.38)	2–18	0.5–3	0.25–0.50	5–70
Ice Aggregates	gamma (μ=7)	6–50	6–15	0.50	0.03–30
Dust-like	lognormal (σ=0.788)	2	1.5	0.25	0.05–0.25
Volcanic dust	lognormal (σ=0.615)	2	4	0.50	0.05–0.30

2.1.2. Ice clouds

Ice clouds are commonly assumed as PSDs of non-spherical ice crystals. In nature, multiple crystal shapes are observed within ice cloud layers depending on the cloud formation conditions, its evolution, and thermodynamic state. Crystal aggregates of eight hexagonal ice columns are considered in this work, whose single scattering single particle radiative properties are described by [41]. A commonly used PSD for ice clouds is the three parameters gamma type distribution, here below written as a function of the maximum dimension of the ice particle D:

$$n(D) = n_0 D^{\mu} e^{-\lambda D} \tag{5}$$

where n_0 is the intercept, or normalization factor, μ is the shape parameter, and λ is the slope parameter. An average value of μ=7 is assumed in this work. A positive value of μ means that the shape of the gamma distribution is of under-exponential type and the maximum of the distribution lies in between the minimum and maximum dimension of the crystals. Since μ is assumed constant and n_0 is a scaling parameter, the different PSDs can be related to the effective dimension only. For non-spherical particles, an effective dimension D_{eff} of the distribution is defined, according to [42], as

$$D_{eff} = \frac{3}{2} \frac{\int_0^{\infty} V(D) n(D) dD}{\int_0^{\infty} A(D) n(D) dD} \tag{6}$$

where A and V are the cross sectional area and the volume of the particle with maximum dimension D. For comparison with liquid water particles, the effective radius of the PSD is defined as $r_{eff} = 0.5D_{eff}$.

Simulations are performed at different r_{eff} values and for ODs ranging from 0.03 to 30, thus spanning from the upper limit of sub-visible cirrus clouds [43] to thick ice layers. The cloud layer top is placed at different heights, whose maximum varies according to the altitude of the Tropopause (light blue bands in Figure 1). All the key parameters concerning ice clouds are reported in Table 2.

2.1.3. Aerosols

Globally, aerosols comprise a large variety of radiative properties due to variation in chemical composition, particle size distributions (often multimodal), and vertical concentration. Even if the most important impact on atmospheric radiances is at short wavelengths (0.3–4 µm) for some types of aerosols their effects at long wavelengths (4–100 µm) is not negligible and must be accounted for in radiative transfer computations. Two types of aerosols are considered for this study: desert dust (dust-like) and volcanic dust. For these cases, the aerosol load in the atmospheric column can reach very high values and significantly influence the local energy balance. Their optical properties are driven by the refractive indices, that are taken from the HITRAN [44] database to cover the 250–1600 cm^{-1} band of the FORUM spectral range. In Figure 2, the imaginary part of the refractive index of volcanic dust [45] and desert dust [46] are compared to those of ice [47] and water [39]. The plot shows that both aerosols are characterized by specific absorption properties along the spectrum with local maxima between 300 and 400 cm^{-1} and at around 1000 cm^{-1}. Their single scattering single particle radiative properties are generated by using the Scattnlay code under the assumption that their shape is spherical. The aerosol PSDs are considered following a lognormal distribution (Equation 1), with a fixed scale parameter for each aerosol type based on average values found in literature. It is assumed that $\sigma_{\text{dust-like}}$=0.788 [48], and $\sigma_{\text{volcanic dust}}$=0.615 [49].

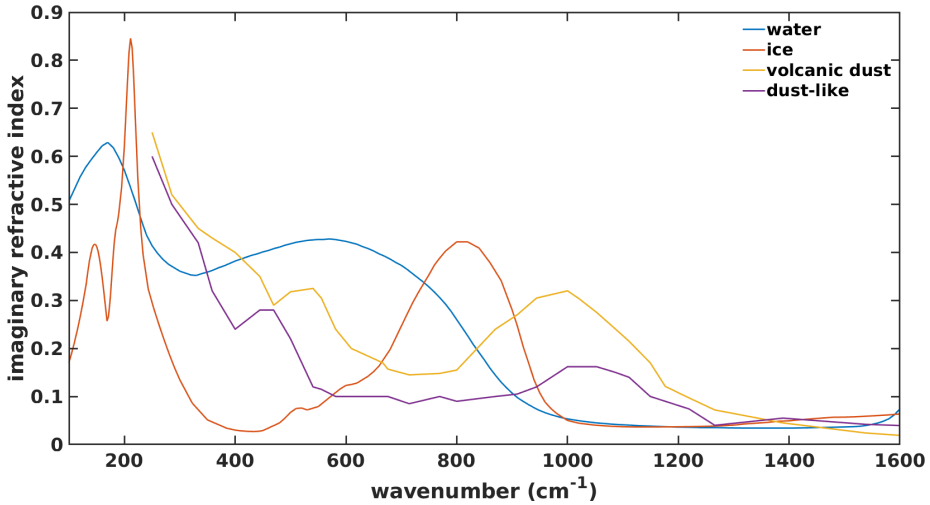

Figure 2: Imaginary part of the refractive indices used for the computation of the cloud and aerosol particle size distributions.

The aerosol contribution is analysed in the low latitude scenario for the dust-like particles, and in the mid latitude scenario in case of volcanic dust. A uniform aerosol layer is considered, whose height is selected according to the work by [50] on typical Saharan aerosol plumes and by [49] on Eyjafjallajökull 2010 eruption. The range of ODs used in the desert dust simulations is based on the values stored in the CAMS database [51, 52] for the month of June 2019 off the Atlantic coast of North Africa, referred to an event of dust transportation assumed as a representative case study. The work about the Eyjafjallajökull 2010 eruption by [53] is used to determine the range of ODs for the volcanic dust simulations. The main aerosol parameters used in the radiative transfer computations are summarized in Table 2.

2.2. Computational methodologies

The accurate solution for the upwelling spectral radiance at far and mid infrared wavelengths in multiple scattering conditions is compared to fast solutions based on scaling methods. The same simulation chain of radiative transfer models (Figure 3) is used for each one of the considered configurations:

- the Full Scattering (FS) that exploits the full functionalities of a numerical algorithm solving the radiative transfer equation in presence of multiple scattering events;

- the Chou Approximation (CA) that scales the absorption properties of the scattering layers by using an hemispheric backscattering function and solves the radiative transfer equation in a pure absorption/emission configuration;

- the Similarity Principle (SP) that is used, as in the CA case, to define scaled absorption properties of the scattering medium emulating the scattering process in a pure absorption/emission approximation.

For the three configurations, the only difference in the whole process concerns the set-up of the radiative transfer solution in the scattering layer, that is, any case, obtained by using the DISORT model [11]. Thus, the same radiative transfer code carries out both full scattering computations, by using all the relevant scattering parameters (FS solution), and approximated scattering computations, by using the clear sky radiative transfer equation based on the apparent optical depths computed in accordance with the Chou approximation or the similarity principle. The use of the same code chain and the same set-up in different configurations, rather than the usage of different codes, avoids the introduction of possible code-dependent systematic errors and thus allows a better assessment of the accuracy of the scaling methodology in comparison to the full scattering solution for different conditions.

Figure 3 provides a flow-chart of the code chain and highlights how the same algorithm is used in different configurations. A more detailed description of the three configurations is provided in the following sections.

2.2.1. Full scattering

The current analysis is based on synthetic spectral radiances generated by the line-by-line radiative transfer model LBLDIS [13], a combination of the AER's LBLRTM [54] and the DISORT [11] routines.

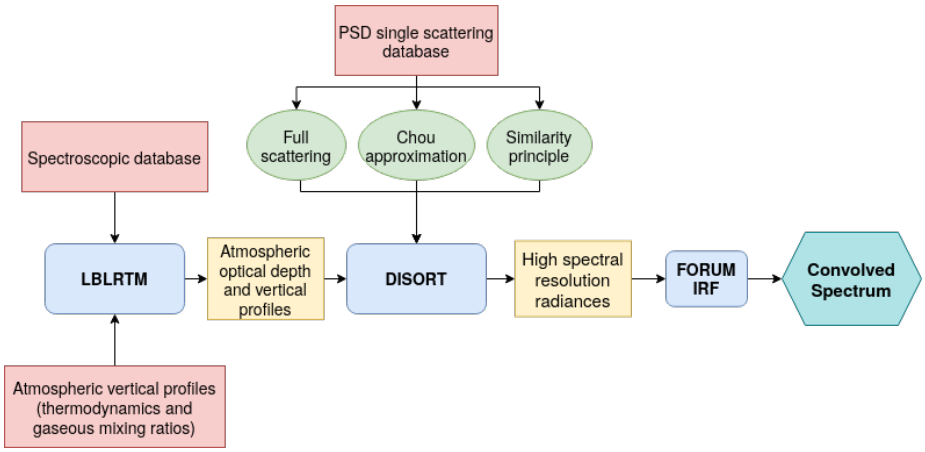

Figure 3: Flow diagram of the code chain used for the radiative transfer simulations. Databases are in red boxes, codes are in blue and outputs are in yellow. The three methodologies are highlighted in green. The final spectrum is a synthetic FORUM-like observation. See text for more details.

LBLRTM is an accurate, flexible, and efficient line-by-line radiative transfer model and includes a recently updated water vapour continuum parameterization (MT_CKD v3.2, [28]) and the spectroscopic database AER v3.6, built from HITRAN 2012 [55]. The LBLRTM v12.7 is used to compute the atmospheric optical depth for each layer of the model (52, from 0 to 80 km), characterized by the vertical profiles provided in Section 2.1.

DISORT is a plane parallel discrete ordinate algorithm for monochromatic unpolarized radiative transfer in non-isothermal, vertically inhomogeneous media. LBLDIS uses the DISORT v2.0, which was compiled using double precision to solve some numerical issues. The LBLRTM outputs and the single scattering PSD properties of clouds and aerosols, described in Section 2.1, are used as input for LBLDIS to compute high spectral resolution radiances.

The high resolution spectra ($\Delta\tilde{\nu}$=0.01 cm^{-1}) are successively convolved with a *sinc* function emulating an ideal FORUM instrumental response function. The final spectral resolution, that is the full width at half maximum of the unapodised instrument spectral sampling function, is set at 0.36 cm^{-1} [56].

The FS solution is obtained using the code chain described in Figure 3 in its full potentialities, meaning that the DISORT routine is run to solve the multiple scattering radiative transfer in presence of cloud or aerosol layers. In this configuration, the required input properties for each scattering layer involve the extinction, absorption and scattering coefficients and the angular description of the phase function of the specific PSD accounted for.

2.3. CA method

According to the Chou approximation [7], the scattering contribution is accounted for by replacing the optical depth (τ) of each atmospheric layer with an *apparent* optical depth for extinction:

$$\tilde{\tau} = (1 - \omega_0)\tau + b\omega_0\tau \tag{7}$$

where ω_0 is the single scattering albedo and b is the mean fraction of radiation that is scattered by the cloud/aerosol particles in the backward hemisphere. The first term on the right-hand side of Equation 7 represents the actual absorption of the layer, and the second term is an additional absorption related to the radiation removed from the beam because of the backscattering processes. The backscattering function b quantifies the hemispheric backscattered radiation and it is formally computed through an integration of the phase function P of the considered PSD. It is defined by [7] (Eq. 10) as

$$b = \frac{1}{2}\int_0^1 d\mu \int_{-1}^0 P(\mu, \mu')d\mu' \tag{8}$$

where μ is the cosine of the zenith angle and the integration limits indicate that the radiation is scattered toward the incoming hemispheric direction. Chou et al. [7] (Eq. 11) provides a polynomial fitting of b through the asymmetry parameter g as

$$b = 1 - \sum_{i=1}^{4} a_i g^{i-1} \tag{9}$$

where the coefficients a_i, reported in Table 3, are jointly retrieved for liquid water and ice PSDs. In particular, the PSD parameters used to derive the latter relation are computed by [7] for a modified gamma distribution of liquid water droplets and for randomly oriented hexagonal ice crystals computed using the outdated method by [57]. Improvements in the b formulation are presented in Section 3.1.

The CA scaling method is obtained by using the code chain shown in Figure 3. In this case, the DISORT routine is run without accounting for scattering processes. The procedure requires to modify the input PSD radiative properties in accordance with Equation 7 to account for the *apparent* optical depth for extinction.

2.3.1. Similarity principle

An approach similar to CA for fast radiative transfer computations is described by [34], based on the application of the similarity relation on ice cloud radiance calculations by [58]. As in CA, the full scattering computation is avoided by considering a pure absorbing/emitting atmosphere with scaled *apparent* optical depth for extinction:

$$\tilde{\tau} = (1 - \omega_0)\tau + \left(\frac{1 - g}{2}\right)\omega_0\tau \tag{10}$$

Similarly to Equation 7, the first term on the right-hand side represents the actual absorption of the layer and the second term is an additional absorption related to the radiation removed from the beam because of the scattering processes. The advantage of the SP with respect to CA consists in depending on the asymmetry parameter in a very simple way, and thus not demanding time consuming computations such as those required for the definition of the backscattering function b.

As in the CA case, the DISORT routine is run without accounting for scattering processes, and by modifying the input PSD radiative properties according to the *apparent* optical depth for extinction of Equation 10.

3. Results

3.1. Accurate computation and parameterization of b

According to [7], the backscattering function b is computed through the polynomial approximations of Equation 9, which accounts for both liquid water and ice clouds. Moreover, as already noticed, the ice particle scattering properties are taken by [57] and thus do not benefit of all the scientific and computational improvements achieved in the last years as those used in this study [41]. An improvement of the CA is presented by accurately computing the b parameter using Equation 8 for the integration of the phase functions of the PSDs, provided with the reference database of optical properties described in Section 2.1. The integration of Equation 8 requires to explicit the dependence of the phase function on the incoming and exiting azimuth angles ϕ' and ϕ:

$$b = \frac{1}{2}\int_0^{2\pi}\frac{1}{2\pi}d\phi\int_0^{2\pi}\frac{1}{2\pi}d\phi'\int_0^1 d\mu\int_{-1}^0 P(\mu,\phi,\mu',\phi')d\mu' \tag{11}$$

A Monte Carlo technique is used, which is a common method for the evaluation of high dimensional integration problems. Given an integration problem:

$$E = \int_{\mathbb{D}} f(x)dx \tag{12}$$

where $\mathbb{D} \subset \mathbb{R}^n$ is the domain of integration, it is possible to prove [59] that a good estimator for E is given by

$$E \simeq \frac{1}{N}\sum_{i=1}^{N}\frac{f(x_i)}{g(x_i)} \tag{13}$$

where $g(x)$ is any probability density function which is normalized on the given domain $\mathbb{D}$, and the N points x_i are randomly sampled from the distribution $g(x)$. For $g(x)$ being a uniform distribution in $\mathbb{D}$, then E can be expressed as

$$E \simeq \frac{V}{N}\sum_{i=1}^{N} f(x_i) \tag{14}$$

where $V = \int_{\mathbb{D}} dx$ and the approximation error is $\propto 1/\sqrt{N}$. Thus, from Equations 11 and 14, b can be computed as

$$b \simeq \frac{1}{2N} \sum_{i=1}^{N} P(\mu_i, \phi_i, \mu_i', \phi_i') \tag{15}$$

being $\mathbb{D} = \{\mu \in [0,1],\ \phi \in [0, 2\pi],\ \mu' \in [-1, 0],\ \phi' \in [0, 2\pi]\}$, and $V = 4\pi^2$. For a sample of randomly oriented particles, the phase function only depends on the cosine of the scattering angle $\cos\theta$. Therefore, Equation 15 can be expressed as

$$b \simeq \frac{1}{2N} \sum_{i=1}^{N} P(\cos\theta_i) \tag{16}$$

where $\cos\theta_i$ is computed from spherical geometry for N quartets of incoming and outgoing directions in the domain $\mathbb{D}$:

$$cos(\theta_i) = \mu_i \mu_i' + (1 - \mu_i^2)^{\frac{1}{2}} (1 - \mu_i'^2)^{\frac{1}{2}} cos(\phi_i' - \phi_i) \tag{17}$$

The results of the Monte Carlo computations of b for liquid water and ice aggregates PSDs are shown, respectively, in the left and right panel of Figure 4 (blue dots) for wavenumbers from 100 to 1600 cm^{-1}. They should be considered as the correct values of b for the liquid water droplets and column aggregate crystals PSDs accounted for in the present study, since they are derived from the explicit computation of the integral reported in Equation 11. In Figure 4, the backscattering functions are plotted as a function of the corresponding asymmetry parameters and compared with the values obtained by using the polynomial parameterization of Equation 9 (black solid line) for the same asymmetry parameter range. As particle size increases, b decreases mostly because of the increasing of the phase function forward lobe (consequently, g increases), that makes the quantity of the energy scattered in the forward hemisphere prevail on the backscattered one.

Note that the coefficients used for Equation 9 are derived by [7] to simulate the b function of both liquid water and ice PSDs, thus, they are representative of average cloudy conditions. Differences among the Monte Carlo b values and

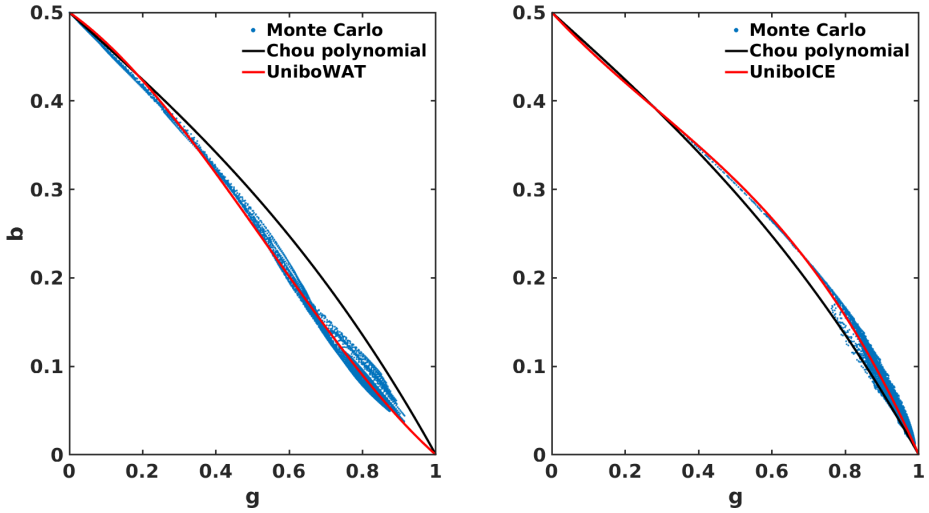

Figure 4: Left panel: Comparison of the backscattering function b versus the asymmetry parameter g of liquid water PSDs for three computation approaches: exact integral using Monte Carlo (blue dots, Equation 16), polynomial by Chou et al. (black line, Equation 9), and polynomial fit with updated coefficients, UniboWAT (red line, Table 3). Right panel: same as left panel, but for ice aggregates PSDs. The updated polynomial fit (red line, Table 3) is called UniboICE.

the Chou parameterization are significant. In particular, Equation 9 provides an overestimation of b for liquid water PSDs and an underestimation of b for ice PSDs composed of column aggregates crystals. The percentage differences between the explicit computation of the backscattering function and the Chou polynomial description can be as high as 80% and 50% for liquid water and ice PSDs, respectively. Such differences in the backscattering function propagate into spectral radiance differences that reach values between 2% and 8% for liquid water and ice clouds, respectively, for the cases considered in this work (see Section 3.3). The use of the updated b functions is thus strongly suggested and it constitutes the adopted solution in this work.

In order to maintain an expression of b as a polynomial function of the asymmetry parameter, so that it would be easier to update existing codes based on the Chou approximation, a fitting procedure is applied to the Monte Carlo values of b for water and ice clouds separately (Table 3). The proposed polynomial expressions are formally identical to that suggested by [7] but improve the accuracy of the computation. They are named UniboWAT when specifically refer to liquid water clouds and UniboICE in case of ice clouds. The UniboWAT and UniboICE are reported in Figure 4 as red curves. The coefficient of determination R^2 is 0.995 for UniboWAT and and 0.989 for UniboICE.

In the present work, the re-scaling methodology is applied by using the exact values of b as computed by means of the Monte Carlo integration described above. The new parameterizations UniboWAT and UniboICE could also be used since the differences on the radiances with respect to using the exact b are negligible.

3.2. Scattering correction term for CA and SP

A preliminary analysis is performed to evaluate the magnitude of the additional term that, summed to the actual absorption $(1 - \omega_0)\tau$, accounts for scattering in the apparent optical depth for extinction, introduced by the approximate methodologies as shown in Equations 7 and 10. Figure 5 compares the re-scaling terms that, once multiplied by τ, are used in the CA ($\omega_0 b$) and in the

Table 3: Coefficients for the polynomial fitting of b versus g. The fits are in the form $b = 1 - \sum_i a_i g^{i-1}$.

Name	Application	a_1	a_2	a_3	a_4
Chou	Liquid water and ice clouds	0.5	0.3738	0.0076	0.1186
UniboWAT	Liquid water clouds	0.5	0.2884	0.5545	−0.3429
UniboICE	Ice aggregates clouds	0.5	0.4452	−0.3189	0.3737

SP ($\omega_0(1-g)/2$) when in presence of a typical liquid water cloud (r_{eff}=10 µm, top panel) and of a typical ice cloud (r_{eff}=30 µm, bottom panel). Note that $\omega_0 b$ is computed using the accurate method described in Section 3.1. Results show that in case of liquid water cloud (upper panel of the Figure) the scaling terms are very similar, especially in the FIR and up to 1000 cm^{-1}. It is thus expected that top of the atmosphere radiance fields generated using the CA or SP method result in similar solutions. In case of ice clouds (lower panel of the Figure), the SP approach provides a lower contribution to the optical depth with respect to the CA along the entire spectrum. Similar behaviour is observed over the whole range of the considered PSDs of ice crystals. Due to a smaller absorption, it is expected that the top of the atmosphere radiance generated using the SP solution is higher than that obtained when the CA configuration is adopted in presence of ice clouds.

3.3. Spectral radiance analysis

Cloud and aerosol properties described in Section 2.1 are used in a wide number of simulations to evaluate the impact of re-scaling methodologies, CA and SP, with respect to the full scattering solution for multiple scenarios.

The level of approximation when using a simplified approach instead of the FS solution is evaluated in terms of spectral radiance differences as

$$\Delta L = L_{\mathrm{X}} - L_{\mathrm{FS}} \tag{18}$$

where X is either CA or SP. Where not explicit, radiances are reported in mW/(m^2 sr cm^{-1}) (hereinafter, radiance units – RU). The radiance differ-

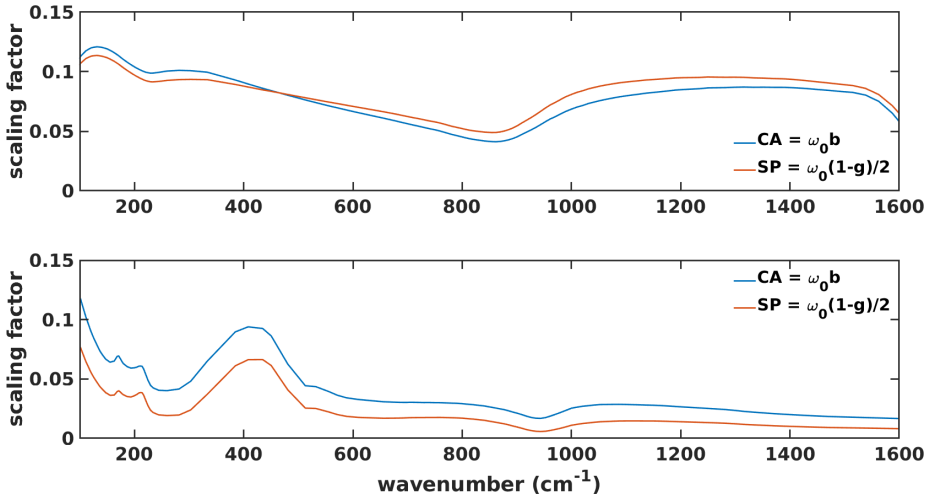

Figure 5: Optical depth re-scaling terms (see legend and text) in case of CA (blue line) and SP (orange) approaches, as a function of wavenumber. Upper panel: liquid water PSD with r_{eff}=10 µm. Bottom panel: ice aggregates PSD with r_{eff}=30 µm.

ences are compared to the noise equivalent spectral radiance (NESR) specified for the FORUM mission, to evaluate the impact of the different simulation methods with a typical observational uncertainty. The FORUM goal NESR (FGN) is 0.4 mW/(m^2 sr cm^{-1}) within the spectral region 200–800 cm^{-1}, and 1.0 mW/(m^2 sr cm^{-1}) outside [56]. Similarly, the differences in terms of spectral brightness temperature (BT) are also evaluated as

$$\Delta BT = BT_{\mathrm{X}} - BT_{\mathrm{FS}} \tag{19}$$

and expressed in Kelvin.

3.3.1. Liquid water clouds

Low-level liquid water cloud spectra are computed for the four geolocations and for multiple values of cloud top height, r_{eff}, and OD as reported in Section 2.1.1. Figure 6 shows an example for a mid latitude cloud layer with OD=15, placed at 1.5 km height. The upper panel shows the FS spectral radiance for five effective radii, whereas the bottom panel shows the difference

ΔL between the radiances computed using the CA and the FS solution for the same conditions. The FORUM noise is highlighted by the grey shaded area for comparison. At small and large wavenumbers, that is below about 350 cm^{-1} and above 1400 cm^{-1}, ΔL is almost null. The main reason is related to the large atmospheric opacity mostly due to the water vapor absorption. Thus, the assumptions on the adopted radiative transfer solution is irrelevant in these spectral regions. Similarly, the strong absorption due to the CO_2 band around 667 cm^{-1} masks the cloud effects on the top of the atmosphere radiance. It is noted that CA always overestimates the computed FS radiance with the only exception of a slight underestimation in the atmospheric window ($\sim$900 cm^{-1}) for large effective radii. In the MIR region, only very small cloud particles ($r_{eff} \simeq 2$ µm) do not allow a satisfactory approximation of the FS solution and the error is about twice the FGN. Significant discrepancies are observed at FIR wavenumbers, with a peak $\Delta L \simeq 3\times$FGN occurring at about 531 cm^{-1}. For the case reported in the Figure, only for $r_{eff} \geq 10$ µm the scaled approximation is within the FGN limit with respect to the FS.

A more complete picture of the level of accuracy of the CA method with respect to the FS solution is provided by Figures 7 and 8. In the Figures, ΔL and ΔBT at 1203 cm^{-1} and 531 cm^{-1} are shown for many atmospheric and water cloud conditions as a function of the cloud OD and r_{eff}. The selected wavenumbers are those where the largest MIR and FIR differences occur between the approximate method and the full scattering solution, in accordance with what shown in Figure 6. The contour lines show ΔL values in mW/(m^2 sr cm^{-1}), while the color scale highlights the ΔBT values only for ΔL larger than the FGN, that is 1.0 mW/(m^2 sr cm^{-1}) at 1203 cm^{-1} and 0.4 mW/(m^2 sr cm^{-1}) at 531 cm^{-1}, delimited by the red contour line. ΔBT smaller than the FORUM noise are in white.

Figure 7 demonstrates that using CA for computing top of the atmosphere radiances in presence of water clouds in the MIR is a valid approximation for most of the atmospheric and cloud conditions. Only in presence of very small PSDs ($r_{eff} \lesssim 5$ µm) differences larger than the FGN are observed. The differ-

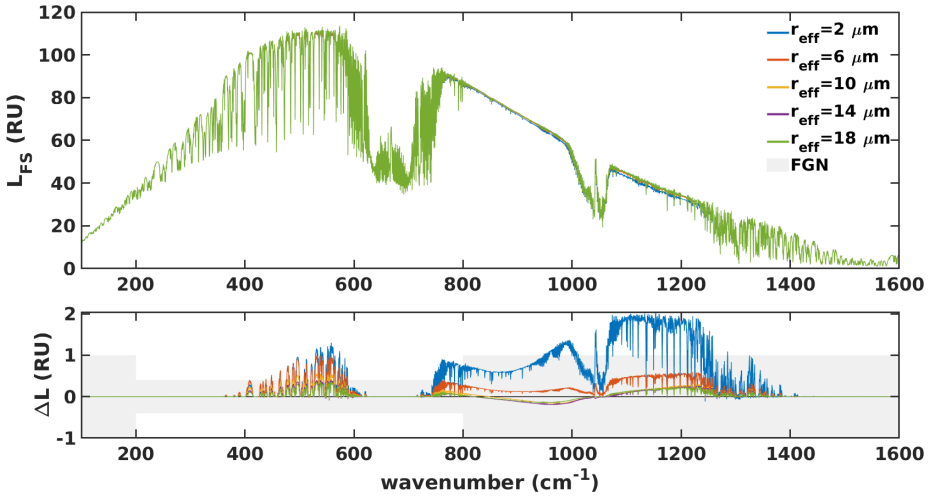

Figure 6: Top panel: top of the atmosphere FORUM spectral radiances computed with the FS approach for a 50°N atmosphere in presence of a liquid water cloud layer, whose top is placed at 1.5 km and with OD=15. Bottom panel: radiance differences between CA and FS approaches for the same clouds as in the top panel. FGN is highlighted by a grey shaded area.

ences are weakly dependent on cloud optical depths and mostly related to water droplets dimensions. Such small effective radii are anyway quite rare. Average liquid water cloud effective radii derived from MODIS AQUA L3 monthly products [60] for the selected geolocations and dates span over the range 11–20 µm.

In terms of radiance differences, the FIR spectral region (Figure 8) is comparable to what found in the MIR. In fact, the level of approximation mostly depends on the considered PSD effective radius. Small effective radii cause a radiance overestimation that is larger than that obtained for the larger radii for each considered scenario. As noted for the MIR, the extent of CA with respect to the FS solution is weakly dependent on cloud OD, and ΔL remains almost constant over the considered OD range. Some variations are noticed for very small ODs and the cause is probably related to environmental conditions that are closer to a single scattering configuration, which is far from the assumption of isotropy that is made in the Chou approximation. Nevertheless, OD value close to unity is a very uncommon situation in case of water clouds. In fact,

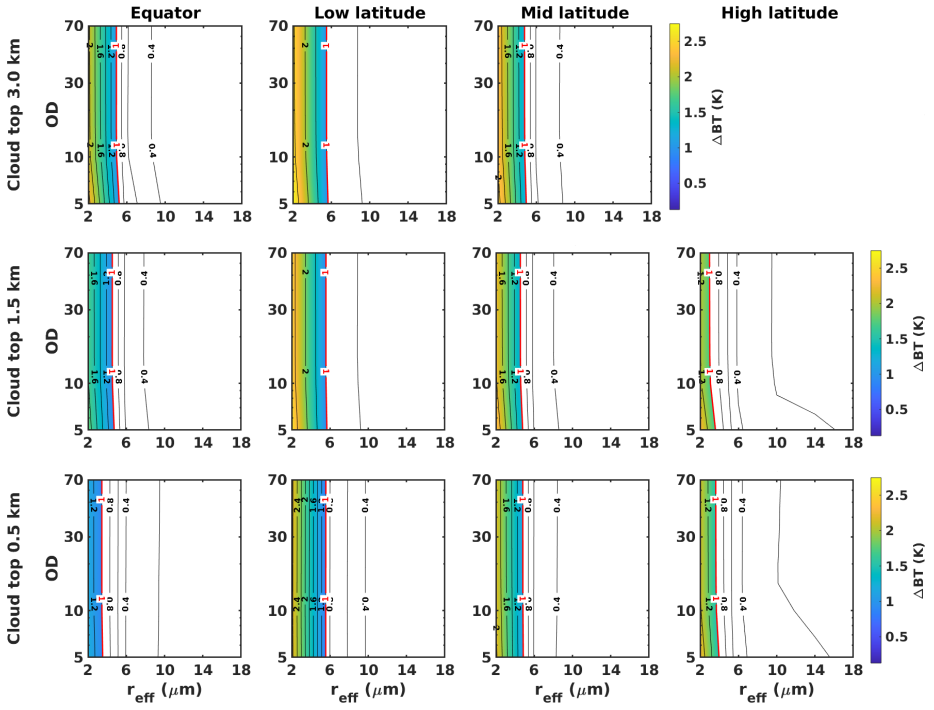

Figure 7: Radiance (ΔL, contour) and brightness temperature (ΔBT, color) differences between CA and FS approaches at 1203 cm^{-1} (MIR), for liquid water clouds. The white color indicates differences below the FORUM noise level, marked by the red contour line. Y-axes are in log scale.

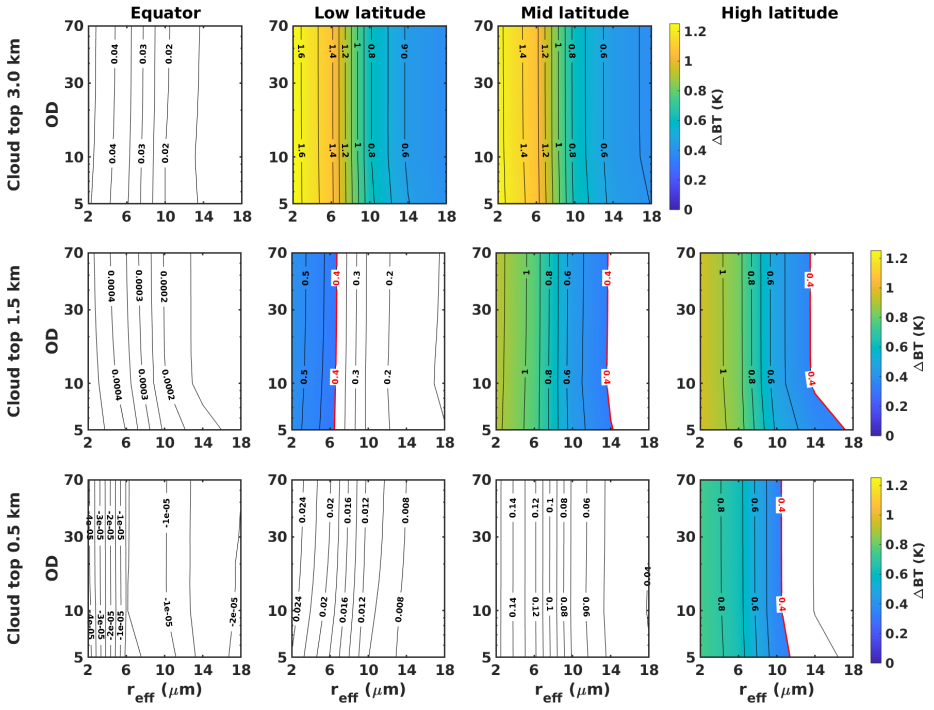

Figure 8: Radiance (ΔL, contour) and brightness temperature (ΔBT, color) differences between CA and FS approaches at 531 cm^{-1} (FIR), for liquid water clouds. The white color indicates differences below the FORUM noise level, marked by the red contour line. Y-axes are in log scale.

Table 4: Precipitable water vapor in the atmospheric column above the case studies cloud top.

	Equator	Low latitude	Mid latitude	High latitude
Cloud top (km)	PWV (mm)	PWV (mm)	PWV (mm)	PWV (mm)
15.0	0.0033	0.0034	–	–
12.0	0.019	0.0089	0.0065	–
8.0	0.28	0.10	0.15	0.016
6.0	–	–	0.54	0.051
3.0	10.4	1.1	1.2	–
1.5	25.1	4.5	2.0	1.3
0.5	38.9	11.4	6.2	2.2

monthly mean optical depths at 900 cm^{-1}, derived from MODIS AQUA L3 products [61] for the same locations and time of the year considered in this study, mostly span over the range 4–18.

At FIR, the simulated radiance differences between re-scaled and exact method are significant for almost all the cases which account for very dry atmospheric conditions. The precipitable water vapor amount above the cloud layers (Table 4) has an attenuating effect on cloud radiances since it is related to the upper atmospheric layer transmissivity. Thus, the higher the PWV above the cloud top level, the lower the radiance difference ΔL. The masking effect becomes very effective for PWV larger than about 4 mm. Thus, radiance differences increase with increasing the cloud top for a fixed latitude, as well as with increasing latitude for the same cloud top height. The CA solution is then accurate when low level clouds and humid conditions are accounted for, and progressively degrades for drier conditions. In these latter cases, CA can provide overestimation, in terms of brightness temperature, of about 1 K at FIR wavenumbers for the worst configurations, that is reached when considering very small water droplets.

As noted in Section 3.2, in case of liquid water clouds the SP approach models

very similar optical depths to those obtained using the CA solution. Since their analysis carries to the same conclusions obtained in the CA–FS case, the results of the comparison between the SP and FS radiances are presented in Appendix A without further comments.

3.3.2. Ice clouds

As in case of liquid water clouds, the spectral radiance differences between the CA method and the FS solution are computed also in presence of ice clouds. One example is provided in Figure 9. In the upper panel of the Figure the top of the atmosphere radiance in presence of a mid latitude cirrus cloud (cloud top placed at 8 km and OD=1) is simulated using the full scattering solution for multiple assumptions on the PSD (r_{eff}). In the lower panel of the same Figure, the spectral radiance differences between the CA and FS solutions are shown for the same cloud cases reported in the upper panel. Results show that the largest residuals are found in two window regions: one in the MIR placed at 1100–1250 cm^{-1} and the other one in the FIR between 350 and 600 cm^{-1}. This last part of the spectrum becomes partially transparent for low concentration of water vapor. Small PWV values are found in the atmospheric column above high level clouds and at high latitudes, as reported in Table 4. In the same spectral region, specifically at about 410 cm^{-1}, a local minimum in the imaginary part of the refractive index of ice is found (see back at Figure 2), meaning that a minimum in the cloud absorption is present and scattering processes become important. Note that the radiance differences in the 350–600 cm^{-1} range are relevant, with respect to the FGN, also for the largest effective radii of the PSDs accounted for.

From the FIR and MIR window bands, two wavenumbers are selected in order to provide an assessment of the level of accuracy of the CA method for multiple atmospheric and ice cloud conditions. With reference to the lower panel of Figure 9, the largest ΔL occurs at 1203 cm^{-1} at MIR and at 410 cm^{-1} at FIR and thus the two wavenumbers are selected as illustrative. Figures 10 and 11 show the ΔL and ΔBT at 1203 cm^{-1} and 410 cm^{-1} for the four considered

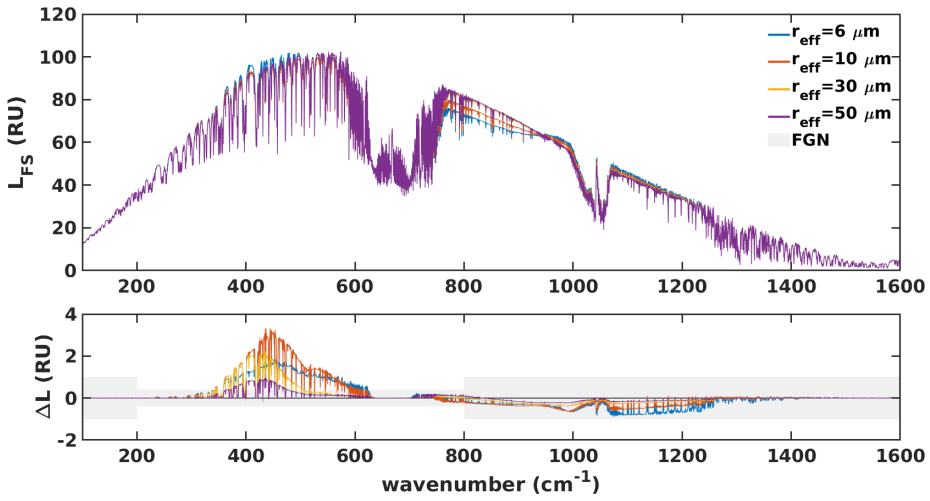

Figure 9: Top panel: top of the atmosphere FORUM spectral radiances computed with the FS approach for a 50°N atmosphere in presence of an ice cloud layer, whose top is placed at 8 km height and with OD=1. Bottom panel: radiance differences between CA and FS approaches for the same clouds as in the top panel. FGN is highlighted by a grey shaded area.

scenarios, at varying cloud altitudes and as a function of the cloud OD and r_{eff}. The OD axis (spanning from 0.03 to 30) is plotted in logarithmic scale so that the radiance and BT differences in case of thin cirrus clouds (OD < 3) are highlighted.

In Figure 10, the radiance and brightness temperature differences at 1203 cm^{-1} are shown. With the exception of cases considering very high clouds (cloud top higher than 12 km) with very small effective radii ($r_{eff} \lesssim 10$) and with OD at around 1, the computed ΔL and ΔBT values are very small. This is proven by the dominating white color in almost all the panels of the Figure, meaning that the CA–FS difference is less than the FORUM noise at that specific wavenumber. The result demonstrates that CA is an accurate approximation in the MIR both in presence of thick ice clouds and in cirrus cloud conditions. Note that for the same location and time of the year, the monthly mean r_{eff} derived from MODIS AQUA L3 products [61] is around 30 µm when in presence of ice clouds (including cirri).

When simulations are performed at 410 cm^{-1}, the CA methodology brings to relevant errors for OD larger than unity, as shown in Figure 11. In the Figure, ΔL and ΔBT values lower than FORUM noise (white areas) are observed for optically thin cirrus clouds almost independently of the assumed r_{eff}. As the cloud OD increases, the accuracy of the CA simulations degrades and the synthetic radiances are overestimated. The overestimation can be of the order of 8–10 K when OD are between 10 and 30, and for small effective radii ($r_{eff} \lesssim 10$). The ones reported in Figure 11 are the largest errors, in terms of radiance or BT, over the whole FORUM spectrum and show that the CA methodology is mostly inadequate to simulate FIR radiances in presence of ice clouds with medium-large optical depths.

What shown in Figure 10 and 11 is obtained for ice clouds with a vertical extent of 0.5 km, corresponding to a single layer in the model. In order to evaluate if computational differences between the full scattering solution and the scaling method may depend on cloud vertical extent, the simulations are repeated for multiple geometric thicknesses of the ice clouds: 1.5, 3.0, and 4.5 km, corresponding to 3, 6, and 9 layers in the model, respectively. The same scenarios and optical properties are considered, with the only difference that the total cloud OD is distributed over a larger vertical extent. An example of the results is reported in Figure 12, corresponding to the scenario at 34°N and to an ice cloud with top altitude placed at 15 km. The simulations account for varying cloud thickness as reported on the top of the plots in the upper row. The Figure shows the radiance differences between simulations performed using the CA and the FS methodologies. The upper and lower row refer to differences in the MIR (at 1203 cm^{-1}) and in the FIR (at 410 cm^{-1}) respectively. It is shown that, for optically thick ice clouds (OD$\geq$3) the assumption on the geometric cloud thickness has a negligible effect on the computed radiance differences, both at MIR and at FIR. For optically thin ice clouds, the ΔL is independent of cloud thickness at MIR and shows very small variations at FIR when assuming a 0.5 km or a geometrically thicker cloud. The magnitude of the ΔL variations due to assumptions on cloud thickness is anyway negligible when compared to

the variation due to cloud optical thickness or particles effective dimensions. In conclusion, the results shown in Figures 10 and 11, obtained for a single layer cloud of 0.5 km, can be assumed as representatives of clouds of any vertical extent.

We noted earlier (Section 3.2) that apparent optical depths for extinction, in case of ice clouds, produced by the SP method are smaller than those obtained by using the CA approximation. Thus, it is expected that upwelling radiances in presence of ice clouds are higher in the SP case than in the CA case. Since the CA solution is shown to overestimates the FS computations, the SP approximation is pejorative for the ice cloud conditions considered in this work. The SP–FS comparisons are reported in Appendix A.

3.3.3. Aerosols

Two different aerosol scenarios are simulated, consisting of a layer of desert dust (dust-like) at low latitudes and a layer of volcanic dust at mid latitudes. The two considered scenarios are case studies for typical desert and volcanic dust concentrations, thus not representative of extreme conditions. The aerosol optical properties are described in Section 2.1 and the layers features summarized in Table 2. First, the spectral radiance differences with respect to the clear sky solution are evaluated to define which are the conditions that makes the aerosol layers detectable. This also allows to quantify the FIR radiance sensitivity to the aeresol properties. Successively, the differences ΔL between the spectral radiances simulated using CA and FS configurations are computed for the observational conditions that provide aerosol signal, with respect to clear sky, larger than the FGN. Figures 13 and 14 show, in their respective upper panels, the differences between the clear sky solution and the aerosol loaded scenarios for dust-like and volcanic particles respectively. Multiple ODs are accounted for, spanning over the observed ranges as discussed in Section 2.1.3. In Figures 13 and 14, the FGN is also plotted and highlighted by the grey shaded area.

With reference to the upper panel of Figure 13, it is noted that the dust-like

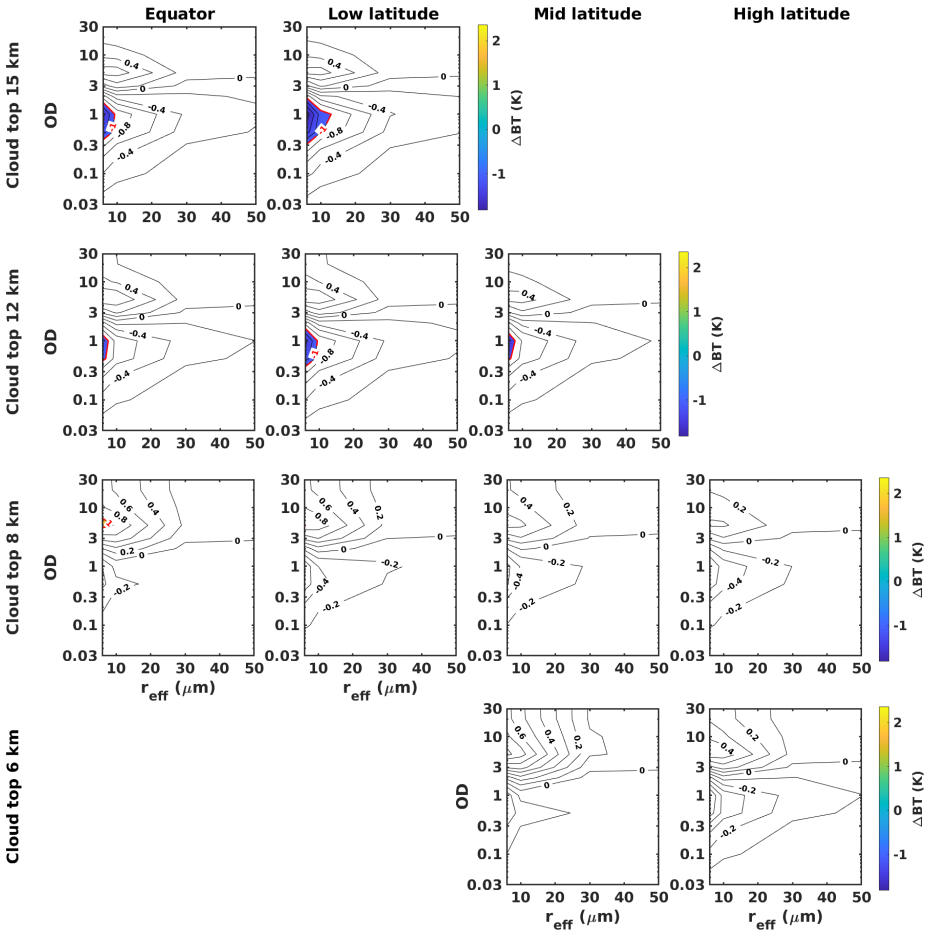

Figure 10: Radiance (ΔL, contour) and brightness temperature (ΔBT, color) differences between CA and FS approaches at 1203 cm^{-1} (MIR), for ice clouds. The white color indicates differences below the FORUM noise level, marked by the red contour line. Y-axes are in log scale.

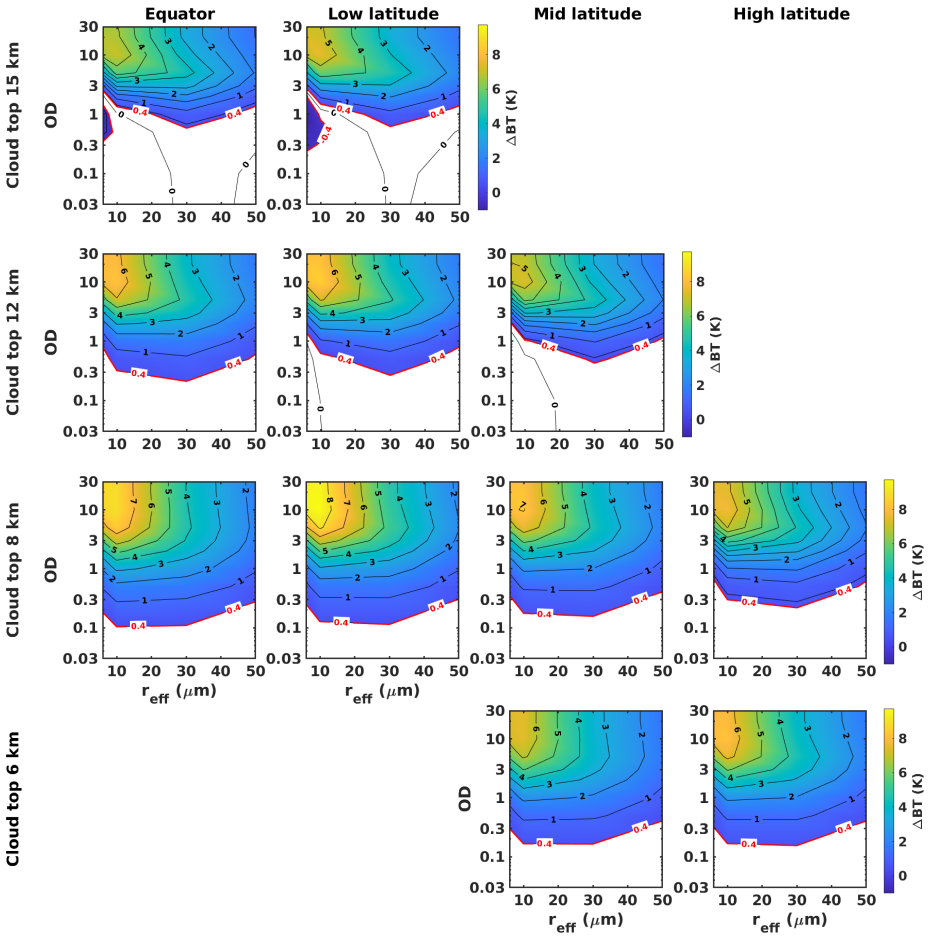

Figure 11: Radiance (ΔL, contour) and brightness temperature (ΔBT, color) differences between CA and FS approaches at 410 cm^{-1} (FIR), for ice clouds. The white color indicates differences below the FORUM noise level, marked by the red contour line. Y-axes are in log scale.

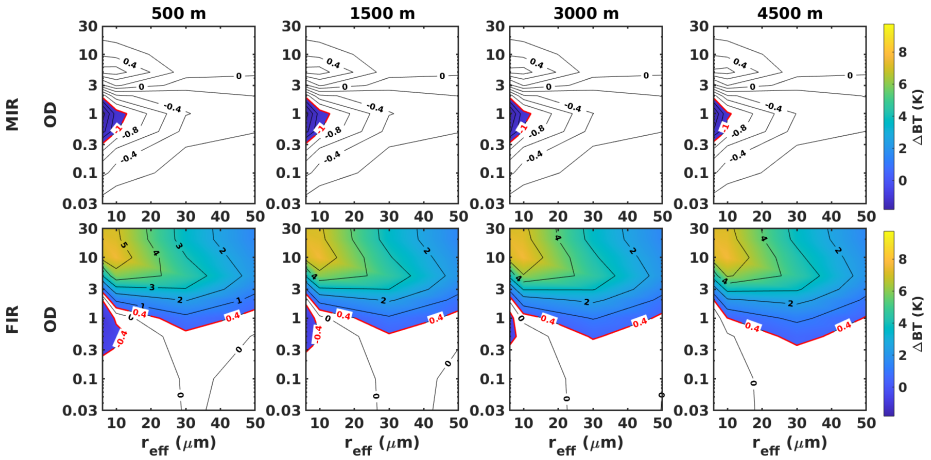

Figure 12: Radiance (ΔL, contour) and brightness temperature (ΔBT, color) differences between CA and FS approaches, at MIR (top panels, 1203 cm^{-1}) and FIR (bottom panels, 410 cm^{-1}) wavenumbers. All the panels refer to the same low latitude scenario (34°N), and to an ice cloud with top placed at 15 km. The cloud geometrical thickness is indicated on the top of the upper panels and ranges from 500 m to 4500 m. The white color indicates differences below the FORUM noise level, marked by the red contour line. Y-axes are in log scale.

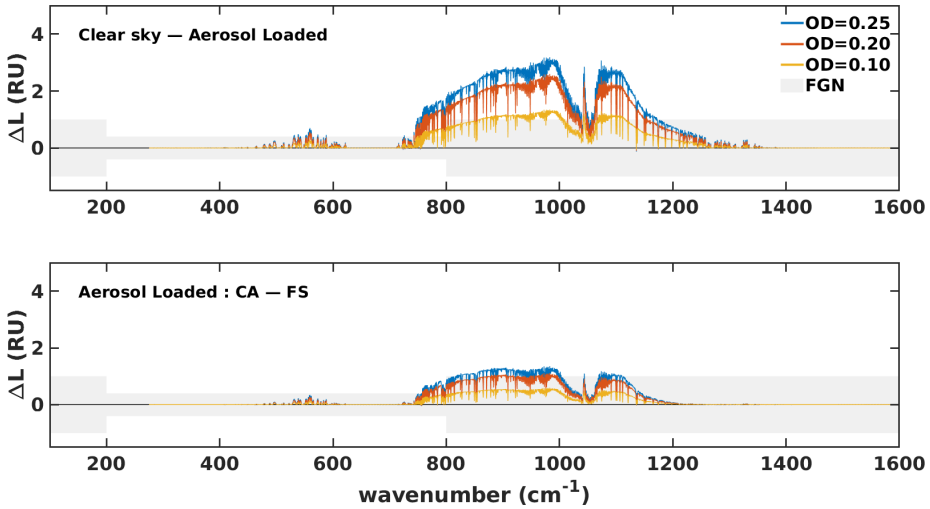

Figure 13: Top panel: spectral differences between FORUM-like observations in clear sky or in presence of an aerosol loaded atmosphere with dust-like particles. Bottom panel: differences between radiances computed using the CA and the FS approaches for the same aerosol cases presented in the upper panel. The simulations are obtained considering a 34°N atmosphere, and r_{eff}=2.0 µm. FGN is highlighted by a grey shaded area.

signal is very small in the FIR part of the spectrum, and only aerosol loads with OD $\gtrsim$ 0.20 are able to produce a signal larger than the FGN with respect to the clear sky. The impact of the dust-like aerosol on clear sky radiances is larger in the MIR where the FGN is exceeded for OD $\gtrsim$ 0.10. The impact of CA re-scaling methodology is thus evaluated only for aerosol scenarios with OD $\geq$ 0.10. The bottom panel of Figure 13 shows the differences ΔL between the radiances computed using the CA and the FS radiative transfer configurations. ΔL is almost null for wavenumbers below about 350 cm^{-1} and above 1400 cm^{-1}, mostly because of the atmospheric opacity and the low impact of the dust-like aerosol on up-welling radiances. At MIR, between 800 and 1000 cm^{-1}, the computational inaccuracies of the CA method become larger than the FGN only for OD larger than 0.2.

The volcanic dust scenario (Figure 14) shows a larger impact on up-welling radiances with respect to the clear sky spectrum when compared to desert dust

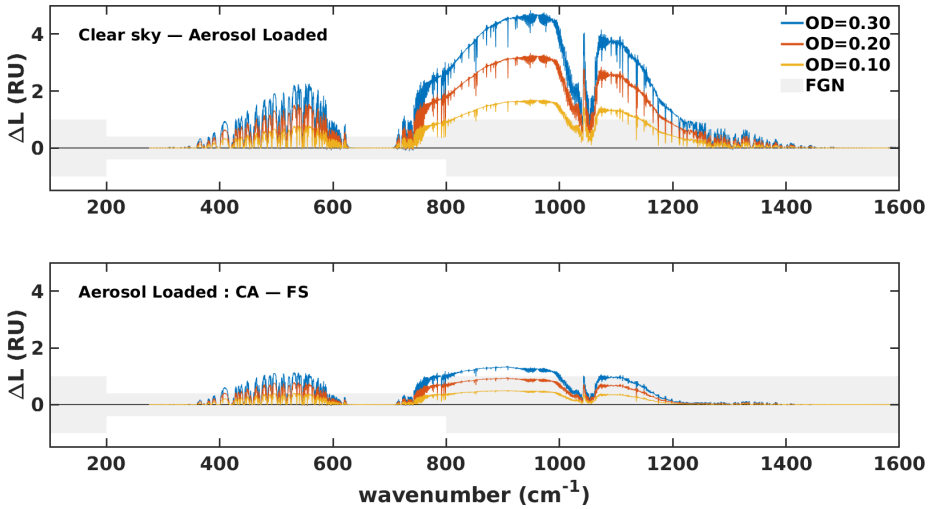

Figure 14: Top panel: spectral differences between FORUM-like observations in clear sky or in presence of an aerosol loaded atmosphere with volcanic dust particles. Bottom panel: differences between radiances computed using the CA and the FS approaches for the same aerosol cases presented in the upper panel. The simulations are obtained considering a 50°N atmosphere, and r_{eff}=2.0 µm. FGN is highlighted by a grey shaded area.

(upper panel of the Figure). The impact is larger than the FGN for OD $\geq$ 0.10 and is not negligible at FIR wavenumbers. Two main reasons lie behind the higher sensitivity of FIR and MIR radiances in presence of volcanic dust. The first one is that the imaginary part of the refractive index of volcanic dust is larger than that of dust-like aerosols in the 250–1400 cm^{-1} range (see back at Figure 2). Since the imaginary part of the refractive index is proportional to the absorption coefficient of the medium, the volcanic aerosol is more absorbing than dust like aerosol for the same assumptions on aerosol concentration and micro-physics. The second reason is linked to the higher altitude and the higher latitudinal location of the volcanic layers. These last conditions imply a dryer and thus more transparent atmosphere. Note also that as the altitude of the volcanic aerosols increases, the peak of the emission from the layer moves towards the smaller wavenumbers due to a smaller temperature of the layer. For the present case, the layer top height is placed at 4.0 km in accordance with

the literature case study taken from [49]. When evaluating the ability of the CA methodology to simulate the up-welling radiances in comparison to the FS method (lower panel of Figure 14) it is noted that at FIR wavenumbers the CA methodology is unsuitable for the volcanic layer with OD larger than 0.2 and produces significant simulation errors, of the order of the half of the change in the signal with respect to the clear sky case.

4. Conclusions

An in-depth assessment of the accuracy of two scaling approaches (the Chou Approximation, CA, and the Similarity Principle, SP) to provide infrared spectral radiance in all-sky conditions has been performed. We have also provided accurate computations of the b-factor used in the CA method, specifically for low level stratiform liquid clouds and ice clouds composed of aggregates crystals. In the CA method, our results are obtained upon such an update. The two approaches (CA and SP) have been compared against Full Scattering (FS) calculations for a wide variety of water and ice clouds, and the results have been analyzed with a focus on the spectral interval 100 to 1600 cm^{-1}, which is the spectral range of the FORUM instrument, the next ESA 9^{th} Earth Explorer. The analysis has also been extended to cover two aerosol types, desert dust and volcanic particles, which can have an effect in the atmospheric window at 10 µm and in the FIR as well. As far as the comparison between the two approaches, CA and SP, in the presence of water clouds, they have shown similar performances. On the contrary, when applied to simulations of cloudy ice fields, the CA has been found to perform better than SP in all conditions which have been analyzed in this study. Our conclusion is that SP is not a valid option to be used and implemented in fast-forward models for ice cloud simulations.

We have found that for radiance calculations, CA approximation for ice and water clouds appears reliable in the MIR, whereas in the FIR it yields acceptable results only in the limit of OD below 0.1–1.0, depending on the atmospheric conditions and cloud altitude. In practice, this does not seem an important

shortcoming for an instrument such as FORUM, which covers from 100 to 1600 cm^1. In the case of aerosols, the situation is more varied. CA scaling methods provide reliable results when the optical depth is below 0.2, and the performance is better for desert dust than for volcanic aerosol.

FORUM is mostly intended to provide spectral radiances aimed at a better comprehensive assessment of the Earth's energy budget. The far-infrared region is governed by many numerous physical processes that can drive climate change (e.g., [8]), but this region is not covered with modern infrared high spectral resolution sensors. However, FORUM has the spectral resolution needed to retrieve the thermodynamical parameters, such as temperature and water vapor mixing ratio profiles, and to perform vertically resolved estimates of cloud optical properties. In particular, it is important to stress that the far-infrared region is particularly suitable for the identification of thin cirrus [33] clouds and the derivation of their physical and optical properties. The same clouds are almost transparent in the mid-infrared. In this respect, our results appear particularly promising for an instrument such as FORUM because they imply that reliable, fast forward models can be developed and used to exploit the synergy between FIR and MIR to retrieve optical properties of water and ice clouds.

As said, modern sensors stop their lower wavenumber to ≈ 640 cm^{-1}, and in fact, all-sky fast forward models have been mostly developed for the mid-infrared (e.g., [15, 16, 17]). Our results open the way to reliable, fast forward models in the FIR, with the quality expected to retrieve liquid and ice water content profiles along with information about the corresponding effective radius. In this respect, we stress that to our knowledge, the results in the FIR are original, and our work provides the first in-depth assessment of Chou approximation in this part of the spectrum. As shown with our study, the CA in the FIR yields acceptable results only in the limit of OD below 0.1–1.0, whereas in the MIR, the approximation can be validly extended to thick clouds. Therefore, a comprehensive analysis of cirrus clouds is possible by resorting to CA-fast radiative transfer schemes, which cover the FIR and MIR spectral ranges, such as FORUM.

In perspective, the CA-based optical depth can be suitably parameterized through look-up tables as a function of LWC/IWC and effective radius. In effect, as a further output of this study, such a parametrization has been already developed for the fast forward model σ-IASI ([16]). An all-sky σ-IASI spectrum over the whole FORUM spectral range (100 to 1600 cm^1) takes $\approx$ 0.5 s to run on a personal computer platform, with Intel(R) Core(TM) i7-1065G7 CPU @ 1.30GHz. The forward model will allow us to check the whole FORUM sensitivity to the optical properties of clouds. Because of its independence of a given forward model, the same parameterization could be embedded in models such as those developed by [15, 17], to name a few, which could open the way to new all-sky fast forward models covering the infrared Earth emitted spectrum in the MIR.

Acknowledgements

The authors would like to thank the Italian Space Agency for the financial support through the project FORUM SCIENZA, the manager of the project Dr. A. Montuori (ASI), and the project PI Dr. L. Palchetti (INO-CNR).

The authors acknowledge the use of computational resources from the parallel computing cluster of the Open Physics Hub (`https://site.unibo.it/openphysicshub/en`) at the Physics and Astronomy Department in Bologna.

The atmospheric profiles in the simulations are generated using Copernicus Climate Change Service information [2020].

The aerosol optical depths in the simulations are generated using Copernicus Atmosphere Monitoring Service Information [2020].

Funding

This research is developed within the Italian Space Agency (ASI) project FORUM SCIENZA Far-infrared Outgoing Radiation Understanding and Monitoring.

Abbreviations

The following abbreviations are used in this manuscript:

BT	Brightness Temperature
CA	Chou Approximation
DISORT	Discrete Ordinate Radiative Transfer
ESA	European Space Agency
FIR	Far InfraRed
FORUM	Far-infrared Outgoing Radiation Understanding and Monitoring
FS	Full Scattering
FGN	FORUM Goal NESR
LBLDIS	LBLRTM + DISORT
LBLRTM	Line-by-Line Radiative Transfer Model

MIR	Mid InfraRed
MOPD	Maximum Optical Path Difference
NESR	Noise Equivalent Spectral Radiance
OD	Optical Depth
PSD	Particle Size Distribution
PWV	Precipitable Water Vapor
RTM	Radiative Transfer Model
RU	Radiance Units
SP	Similarity Principle
SST	Sea Surface Temperature

Appendix A.

Radiance (ΔL, contour plot) and brightness temperature (ΔBT, color scale) differences between SP and FS are shown for liquid water clouds at MIR and FIR wavenumbers in Figure A.15 and A.16, respectively. Results for ice clouds are shown in Figure A.17 and A.18.

References

[1] K. Liou, An introduction to atmospheric radiation, Academic Press, Amsterdam Boston, 2002.

[2] W. Zdunkowski, T. Trautmann, A. Bott, Radiation in the Atmopshere: A Course in Theoretical Meteorology, Cambridge University Press, Cambridge, 2007.

[3] F. Zhang, Y.-N. Shi, K. Wu, J. Li, W. Li, Atmospheric radiative transfer parameterizations, in: L.-M. Ma, Z. Chang-Jiang, F. Zhang (Eds.), Understanding of Atmospheric Systems with Efficient Numerical Methods for Observation and Prediction, IntechOpen, Rijeka, 2019, Ch. 6, pp. 87–102. doi:10.5772/intechopen.82122.
URL https://doi.org/10.5772/intechopen.82122

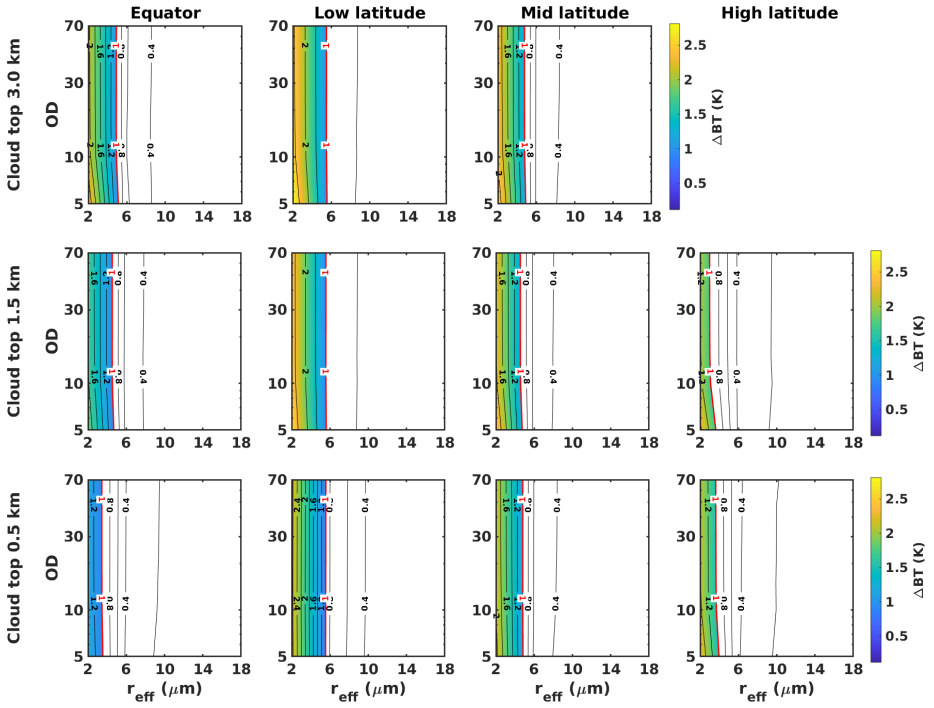

Figure A.15: Same as Figure 7, but for SP.

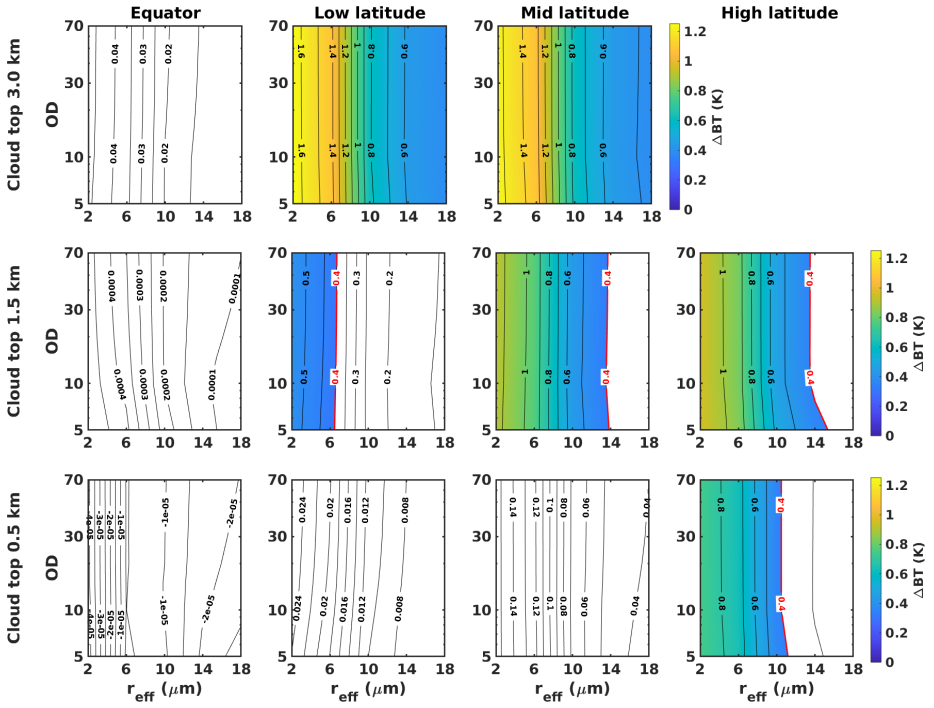

Figure A.16: Same as Figure 8, but for SP.

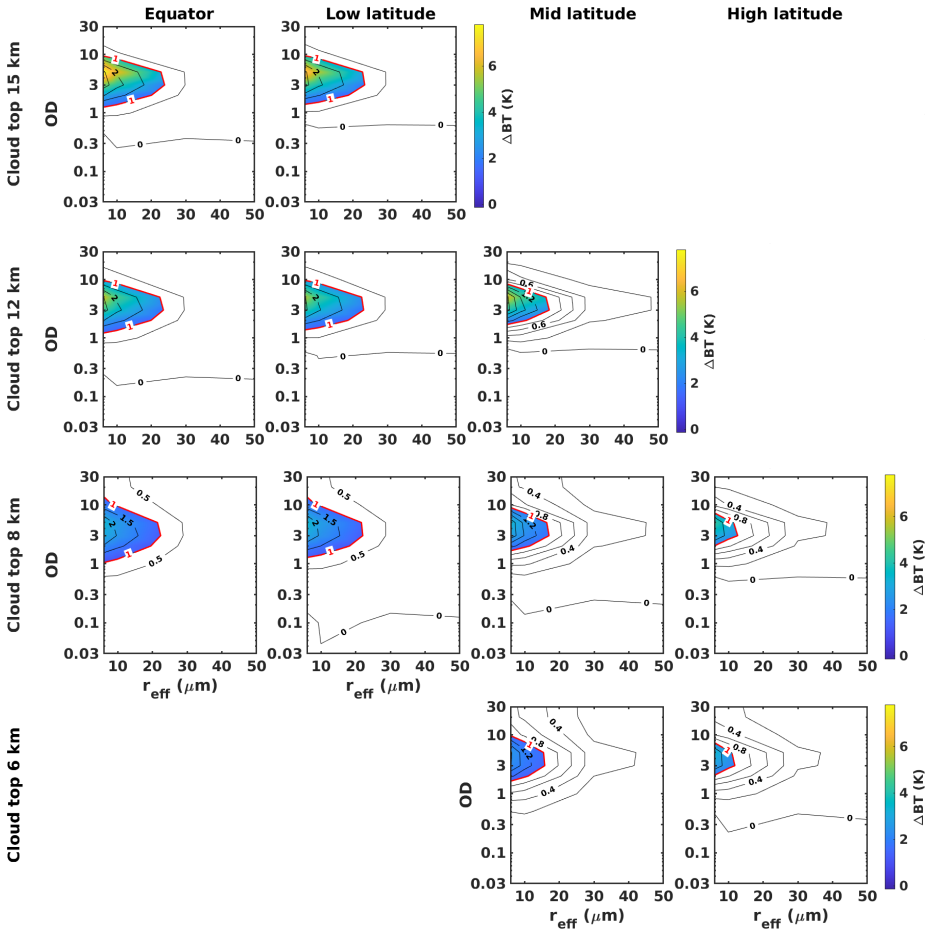

Figure A.17: Same as Figure 10, but for SP.

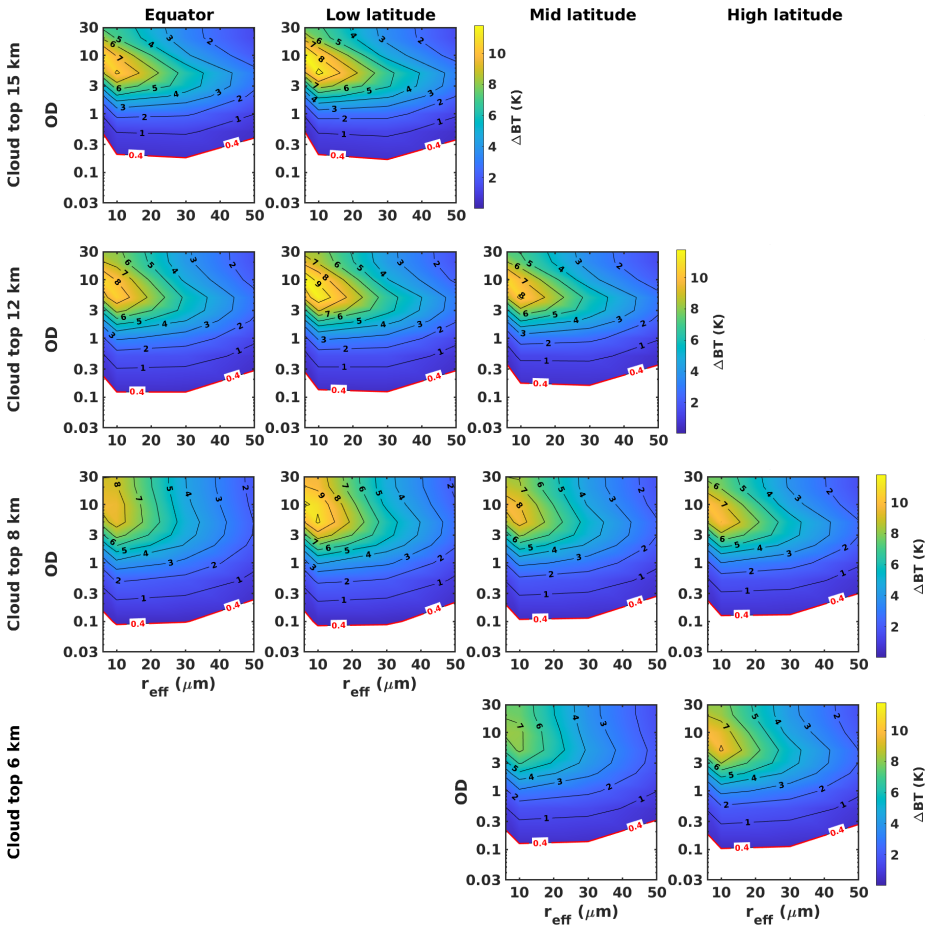

Figure A.18: Same as Figure 11, but for SP.

[4] J. Eyre, A fast radiative transfer model for satellite sounding systems, Technical memorandum 176, ECMWF, Shinfield Park, Reading (03 1991). doi:10.21957/xsg8d92y3.
URL https://www.ecmwf.int/node/9329

[5] M. Matricardi, F. Chevallier, G. Kelly, J.-N. Thépaut, An improved general fast radiative transfer model for the assimilation of radiance observations, Quarterly Journal of the Royal Meteorological Society 130 (596) (2004) 153–173. arXiv:https://onlinelibrary.wiley.com/doi/pdf/10.1256/qj.02.181, doi:https://doi.org/10.1256/qj.02.181.
URL https://onlinelibrary.wiley.com/doi/abs/10.1256/qj.02.181

[6] IPCC, panel, Climate Change 2013: The Physical Science Basis. Contribution of Working Group 1 to the Fifth Assessment Report of the Intergovernmental Panel on Climate Change, Cambridge University Press, Cambridge, 2013.

[7] M.-D. Chou, K.-T. Lee, S.-C. Tsay, Q. Fu, Parameterization for Cloud Longwave Scattering for Use in Atmospheric Models., Journal of Climate 12 (1) (1999) 159–169. doi:10.1175/1520-0442-12.1.159.

[8] L. Palchetti, H. Brindley, R. Bantges, S. A. Buehler, C. Camy-Peyret, B. Carli, U. Cortesi, S. Del Bianco, G. Di Natale, B. M. Dinelli, D. Feldman, X. L. Huang, L. C.-Labonnote, Q. Libois, T. Maestri, M. G. Mlynczak, J. E. Murray, H. Oetjen, M. Ridolfi, M. Riese, J. Russell, R. Saunders, C. Serio, FORUM: unique far-infrared satellite observations to better understand how Earth radiates energy to space, Bulletin of the American Meteorological Society (2020) 1–52arXiv:https://journals.ametsoc.org/bams/article-pdf/doi/10.1175/BAMS-D-19-0322.1/4990048/bamsd190322.pdf, doi:10.1175/BAMS-D-19-0322.1.
URL https://doi.org/10.1175/BAMS-D-19-0322.1

[9] T. Marke, K. Ebell, U. Löhnert, D. D. Turner, Statistical retrieval

of thin liquid cloud microphysical properties using ground-based infrared and microwave observations, Journal of Geophysical Research: Atmospheres 121 (24) (2016) 14,558–14,573. arXiv:https://agupubs.onlinelibrary.wiley.com/doi/pdf/10.1002/2016JD025667, doi:https://doi.org/10.1002/2016JD025667.
URL https://agupubs.onlinelibrary.wiley.com/doi/abs/10.1002/2016JD025667

[10] P. Yang, S. Hioki, M. Saito, C.-P. Kuo, B. Baum, K.-N. Liou, A Review of Ice Cloud Optical Property Models for Passive Satellite Remote Sensing, Atmosphere 9 (12) (2018) 499. doi:10.3390/atmos9120499.

[11] K. Stamnes, S. C. Tsay, K. Jayaweera, W. Wiscombe, Numerically stable algorithm for discrete-ordinate-method radiative transfer in multiple scattering and emitting layered media, Applied Optics 27 (1988) 2502–2509. doi:10.1364/AO.27.002502.

[12] S. A. Clough, M. J. Iacono, J.-L. Moncet, Line-by-Line Calculations of Atmospheric Fluxes and Cooling Rates: Application to Water Vapor, Journal of Geophysical Research (Atmospheres) 97 (D14) (1992) 15,761–15,785. doi:10.1029/92JD01419.

[13] D. D. Turner, S. A. Ackerman, B. A. Baum, H. E. Revercomb, P. Yang, Cloud Phase Determination Using Ground-Based AERI Observations at SHEBA., Journal of Applied Meteorology 42 (6) (2003) 701–715. doi:10.1175/1520-0450(2003)042<0701:CPDUGA>2.0.CO;2.

[14] A. Heidinger, Y. Li, B. Baum, R. Holz, S. Platnick, P. Yang, Retrieval of cirrus cloud optical depth under day and night conditions from modis collection 6 cloud property data, Remote Sensing 7 (6) (2015) 7257–7271. doi:10.3390/rs70607257.
URL http://dx.doi.org/10.3390/rs70607257

[15] M. Matricardi, R. Saunders, Fast radiative transfer model for simulation of infrared atmospheric sounding interferometer radiances, Appl. Opt. 38 (27)

(1999) 5679–5691. doi:10.1364/AO.38.005679.
URL http://ao.osa.org/abstract.cfm?URI=ao-38-27-5679

[16] U. Amato, G. Masiello, C. Serio, M. Viggiano, The σ-iasi code for the calculation of infrared atmospheric radiance and its derivatives, Environmental Modelling & Software 17 (7) (2002) 651 – 667. doi:https://doi.org/10.1016/S1364-8152(02)00027-0.
URL http://www.sciencedirect.com/science/article/pii/S1364815202000270

[17] S. DeSouza-Machado, L. L. Strow, A. Tangborn, X. Huang, X. Chen, X. Liu, W. Wu, Q. Yang, Single-footprint retrievals for airs using a fast twoslab cloud-representation model and the sarta all-sky infrared radiative transfer algorithm, Atmospheric Measurement Techniques 11 (1) (2018) 529–550. doi:10.5194/amt-11-529-2018.
URL https://amt.copernicus.org/articles/11/529/2018/

[18] M. Matricardi, The inclusion of aerosols and clouds in rtiasi, the ecmwf fast radiative transfer model for the infrared atmospheric sounding interferometer, Technical memorandum 474, ECMWF, Shinfield Park, Reading, corrected version posted on December 2012 (07 2005). doi:10.21957/1krvb28ql.
URL https://www.ecmwf.int/node/11020

[19] S. Heilliette, L. Garand, A practical approach for the assimilation of cloudy infrared radiances and its evaluation using airs simulated observations, Atmosphere-Ocean 45 (4) (2007) 211–225. arXiv:https://doi.org/10.3137/ao.450403, doi:10.3137/ao.450403.
URL https://doi.org/10.3137/ao.450403

[20] G. Liuzzi, G. Masiello, C. Serio, D. Meloni, C. Di Biagio, P. Formenti, Consistency of dimensional distributions and refractive indices of desert dust measured over Lampedusa with IASI radiances, Atmospheric Measurement Techniques 10 (2) (2017) 599–615. doi:10.5194/amt-10-599-2017.

[21] G. Liuzzi, M. G. Blasi, G. Masiello, C. Serio, S. Venafra, All-sky radiative transfer calculations for IASI and IASI-NG: The σ-IASI-as code, in: Radiation Processes in the Atmosphere and Ocean, Vol. 1810 of American Institute of Physics Conference Series, 2017, p. 040004. doi:10.1063/1.4975506.

[22] R. Saunders, J. Hocking, E. Turner, P. Rayer, D. Rundle, P. Brunel, J. Vidot, P. Roquet, M. Matricardi, A. Geer, N. Bormann, C. Lupu, An update on the RTTOV fast radiative transfer model (currently at version 12), Geoscientific Model Development 11 (7) (2018) 2717–2737. doi:10.5194/gmd-11-2717-2018.

[23] H. H. Aumann, X. Chen, E. Fishbein, A. Geer, S. Havemann, X. Huang, X. Liu, G. Liuzzi, S. DeSouza-Machado, E. M. Manning, G. Masiello, M. Matricardi, I. Moradi, V. Natraj, C. Serio, L. Strow, J. Vidot, R. Chris Wilson, W. Wu, Q. Yang, Y. L. Yung, Evaluation of Radiative Transfer Models With Clouds, Journal of Geophysical Research (Atmospheres) 123 (11) (2018) 6142–6157. doi:10.1029/2017JD028063.

[24] J. Harries, B. Carli, R. Rizzi, C. Serio, M. Mlynczak, L. Palchetti, T. Maestri, H. Brindley, G. Masiello, The Far-infrared Earth, Reviews of Geophysics 46 (4) (2008) RG4004. doi:10.1029/2007RG000233.

[25] M. G. Mlynczak, D. G. Johnson, H. Latvakoski, K. Jucks, M. Watson, D. P. Kratz, G. Bingham, W. A. Traub, S. J. Wellard, C. R. Hyde, X. Liu, First light from the Far-Infrared Spectroscopy of the Troposphere (FIRST) instrument, Geophysical Research Letters 33 (7) (2006) L07704. doi:10.1029/2005GL025114.

[26] R. Bhawar, G. Bianchini, A. Bozzo, M. Cacciani, M. R. Calvello, M. Carlotti, F. Castagnoli, V. Cuomo, P. Di Girolamo, T. Di Iorio, L. Di Liberto, A. di Sarra, F. Esposito, G. Fiocco, D. Fuà, G. Grieco, T. Maestri, G. Masiello, G. Muscari, L. Palchetti, E. Papand rea, G. Pavese, R. Restieri,

R. Rizzi, F. Romano, C. Serio, D. Summa, G. Todini, E. Tosi, Spectrally resolved observations of atmospheric emitted radiance in the H_2O rotation band, Geophysical Research Letters 35 (4) (2008) L04812. doi:10.1029/2007GL032207.

[27] C. Serio, G. Masiello, F. Esposito, P. di Girolamo, T. di Iorio, L. Palchetti, G. Bianchini, G. Muscari, G. Pavese, R. Rizzi, B. Carli, V. Cuomo, Retrieval of foreign-broadened water vapor continuum coefficients from emitted spectral radiance in the H_2O rotational band from 240 to 590 cmˆ1, Optics Express 16 (20) (2008) 15816. doi:10.1364/OE.16.015816.

[28] E. J. Mlawer, V. H. Payne, J. L. Moncet, J. S. Delamere, M. J. Alvarado, D. C. Tobin, Development and recent evaluation of the MT_CKD model of continuum absorption, Philosophical Transactions of the Royal Society of London Series A 370 (1968) (2012) 2520–2556. doi:10.1098/rsta.2011.0295.

[29] D. D. Turner, E. J. Mlawer, G. Bianchini, M. P. Cadeddu, S. Crewell, J. S. Delamere, R. O. Knuteson, G. Maschwitz, M. Mlynczak, S. Paine, L. Palchetti, D. C. Tobin, Ground-based high spectral resolution observations of the entire terrestrial spectrum under extremely dry conditions, Geophysical Research Letters 39 (10) (2012) L10801. doi:10.1029/2012GL051542.

[30] R. Rizzi, L. Palchetti, B. Carli, R. Bonsignori, J. E. Harries, J. Leotin, S. C. Peskett, C. Serio, A. Sutera, Feasibility of the spaceborne radiation explorer in the far infrared (refir), Proc.SPIE 4485 (2002) 4485 – 4485 – 8. doi:10.1117/12.454252.
URL https://doi.org/10.1117/12.454252

[31] B. A. Wielicki, D. F. Young, M. G. Mlynczak, K. J. Thome, S. Leroy, J. Corliss, J. G. Anderson, C. O. Ao, R. Bantges, F. Best, K. Bowman, H. Brindley, J. J. Butler, W. Collins, J. A. Dykema, D. R. Doelling, D. R. Feldman, N. Fox, X. Huang, R. Holz, Y. Huang, Z. Jin, D. Jennings,

D. G. Johnson, K. Jucks, S. Kato, D. B. Kirk-Davidoff, R. Knuteson, G. Kopp, D. P. Kratz, X. Liu, C. Lukashin, A. J. Mannucci, N. Phojanamongkolkij, P. Pilewskie, V. Ramaswamy, H. Revercomb, J. Rice, Y. Roberts, C. M. Roithmayr, F. Rose, S. Sandford, E. L. Shirley, W. L. Smith, B. Soden, P. W. Speth, W. Sun, P. C. Taylor, D. Tobin, X. Xiong, Achieving climate change absolute accuracy in orbit, Bulletin of the American Meteorological Society 94 (10) (01 Oct. 2013) 1519 – 1539. doi:10.1175/BAMS-D-12-00149.1.
URL https://journals.ametsoc.org/view/journals/bams/94/10/bams-d-12-00149.1.xml

[32] T. Maestri, R. Rizzi, E. Tosi, P. Veglio, L. Palchetti, G. Bianchini, P. Di Girolamo, G. Masiello, C. Serio, D. Summa, Analysis of cirrus cloud spectral signatures in the far infrared, Journal of Quantitative Spectroscopy and Radiative Transfer 141 (2014) 49–64. doi:10.1016/j.jqsrt.2014.02.030.

[33] T. Maestri, W. Cossich, I. Sbrolli, Cloud identification and classification from high spectral resolution data in the far infrared and mid-infrared, Atmospheric Measurement Techniques 12 (7) (2019) 3521–3540. doi:10.5194/amt-12-3521-2019.

[34] G. Tang, P. Yang, G. W. Kattawar, X. Huang, E. J. Mlawer, B. A. Baum, M. D. King, Improvement of the Simulation of Cloud Longwave Scattering in Broadband Radiative Transfer Models, Journal of Atmospheric Sciences 75 (7) (2018) 2217–2233. doi:10.1175/JAS-D-18-0014.1.

[35] H. Hersbach, B. Bell, P. Berrisford, S. Hirahara, A. Horányi, J. Muñoz-Sabater, J. Nicolas, C. Peubey, R. Radu, D. Schepers, A. Simmons, C. Soci, S. Abdalla, X. Abellan, G. Balsamo, P. Bechtold, G. Biavati, J. Bidlot, M. Bonavita, G. De Chiara, P. Dahlgren, D. Dee, M. Diamantakis, R. Dragani, J. Flemming, R. Forbes, M. Fuentes, A. Geer, L. Haimberger, S. Healy, R. Hogan, E. Hólm, M. Janisková, S. Keeley, P. Laloyaux,

P. Lopez, C. Lupu, G. Radnoti, P. de Rosnay, I. Rozum, F. Vamborg, S. Villaume, J.-N. Thépaut, Complete era5: Fifth generation of ecmwf atmospheric reanalyses of the global climate. copernicus climate change service (c3s) data store (cds), (Accessed on 13-07-2020) (2017).

[36] J. J. Remedios, R. J. Leigh, A. M. Waterfall, D. P. Moore, H. Sembhi, I. Parkes, J. Greenhough, M. P. Chipperfield, D. Hauglustaine, MIPAS reference atmospheres and comparisons to V4.61/V4.62 MIPAS level 2 geophysical data sets, Atmospheric Chemistry & Physics Discussions 7 (4) (2007) 9973–10017.

[37] X. Huang, X. Chen, D. K. Zhou, X. Liu, An Observationally Based Global Band-by-Band Surface Emissivity Dataset for Climate and Weather Simulations, Journal of Atmospheric Sciences 73 (9) (2016) 3541–3555. doi:10.1175/JAS-D-15-0355.1.

[38] O. Peña, U. Pal, Scattering of electromagnetic radiation by a multilayered sphere, Computer Physics Communications 180 (11) (2009) 2348–2354. doi:10.1016/j.cpc.2009.07.010.

[39] H. D. Downing, D. Williams, Optical constants of water in the infrared, Journal of Geophysical Research 80 (12) (1975) 1656–1661. doi:10.1029/JC080i012p01656.

[40] N. L. Miles, J. Verlinde, E. E. Clothiaux, Cloud Droplet Size Distributions in Low-Level Stratiform Clouds., Journal of Atmospheric Sciences 57 (2) (2000) 295–311. doi:10.1175/1520-0469(2000)057<0295:CDSDIL>2.0.CO;2.

[41] P. Yang, L. Bi, B. A. Baum, K.-N. Liou, G. W. Kattawar, M. I. Mishchenko, B. Cole, Spectrally consistent scattering, absorption, and polarization properties of atmospheric ice crystals at wavelengths from 0.2 to 100 µm, Journal of the Atmospheric Sciences 70 (1) (2013) 330–347. arXiv:https://doi.org/10.1175/JAS-D-12-039.1, doi:10.1175/JAS-D-12-039.1.
URL https://doi.org/10.1175/JAS-D-12-039.1

[42] J. S. Foot, Some observations of the optical properties of clouds. I: Stratocumulus, Quarterly Journal of the Royal Meteorological Society 114 (479) (1988) 129–144. doi:10.1002/qj.49711447907.

[43] K. Sassen, G. C. Dodd, Haze Particle Nucleation Simulations in Cirrus Clouds, and Applications for Numerical and Lidar Studies., Journal of Atmospheric Sciences 46 (19) (1989) 3005–3014. doi:10.1175/1520-0469(1989)046<3005:HPNSIC>2.0.CO;2.

[44] I. E. Gordon, L. S. Rothman, C. Hill, R. V. Kochanov, Y. Tan, P. F. Bernath, M. Birk, V. Boudon, A. Campargue, K. V. Chance, B. J. Drouin, J. M. Flaud, R. R. Gamache, J. T. Hodges, D. Jacquemart, V. I. Perevalov, A. Perrin, K. P. Shine, M. A. H. Smith, J. Tennyson, G. C. Toon, H. Tran, V. G. Tyuterev, A. Barbe, A. G. Császár, V. M. Devi, T. Furtenbacher, J. J. Harrison, J. M. Hartmann, A. Jolly, T. J. Johnson, T. Karman, I. Kleiner, A. A. Kyuberis, J. Loos, O. M. Lyulin, S. T. Massie, S. N. Mikhailenko, N. Moazzen-Ahmadi, H. S. P. Müller, O. V. Naumenko, A. V. Nikitin, O. L. Polyansky, M. Rey, M. Rotger, S. W. Sharpe, K. Sung, E. Starikova, S. A. Tashkun, J. V. e. Auwera, G. Wagner, J. Wilzewski, P. Wcisło, S. Yu, E. J. Zak, The HITRAN2016 molecular spectroscopic database, Journal of Quantitative Spectroscopy & Radiative Transfer 203 (2017) 3–69. doi:10.1016/j.jqsrt.2017.06.038.

[45] F. E. Volz, Infrared optical constants of ammonium sulfate, Sahara dust, volcanic pumice, and fly ash, Applied Optics 12 (3) (1973) 564. doi:10.1364/AO.12.000564.

[46] F. E. Volz, Infrared refractive index of atmospheric aerosol substances, Applied Optics 11 (4) (1972) 755. doi:10.1364/AO.11.000755.

[47] S. G. Warren, R. E. Brandt, Optical constants of ice from the ultraviolet to the microwave: A revised compilation, Journal of Geophysical Research (Atmospheres) 113 (D14) (2008) D14220. doi:10.1029/2007JD009744.

[48] M. Hess, P. Koepke, I. Schult, Optical Properties of Aerosols and Clouds: The Software Package OPAC., Bulletin of the American Meteorological Society 79 (5) (1998) 831–844. doi:10.1175/1520-0477(1998)079<0831:OPOAAC>2.0.CO;2.

[49] B. Johnson, K. Turnbull, P. Brown, R. Burgess, J. Dorsey, A. J. Baran, H. Webster, J. Haywood, R. Cotton, Z. Ulanowski, E. Hesse, A. Woolley, P. Rosenberg, In situ observations of volcanic ash clouds from the FAAM aircraft during the eruption of Eyjafjallajökull in 2010, Journal of Geophysical Research (Atmospheres) 117 (D20) (2012) D00U24. doi:10.1029/2011JD016760.

[50] J. H. Joseph, O. Yaron, E. Yaroslavich, P. Israelevich, I. Koren, Y. Yair, A. Devir, P. Kischa, Determination of most probable height of desert dust aerosol layer from space, Journal of Geophysical Research (Atmospheres) 113 (D20) (2008) D20S93. doi:10.1029/2007JD009646.

[51] A. Benedetti, J.-J. Morcrette, O. Boucher, A. Dethof, R. J. Engelen, M. Fisher, H. Flentje, N. Huneeus, L. Jones, J. W. Kaiser, S. Kinne, A. Mangold, M. Razinger, A. J. Simmons, M. Suttie, Aerosol analysis and forecast in the european centre for medium-range weather forecasts integrated forecast system: 2. data assimilation, Journal of Geophysical Research: Atmospheres 114 (D13) (2009). arXiv:https://agupubs.onlinelibrary.wiley.com/doi/pdf/10.1029/2008JD011115, doi:https://doi.org/10.1029/2008JD011115. URL https://agupubs.onlinelibrary.wiley.com/doi/abs/10.1029/2008JD011115

[52] J.-J. Morcrette, O. Boucher, L. Jones, D. Salmond, P. Bechtold, A. Beljaars, A. Benedetti, A. Bonet, J. W. Kaiser, M. Razinger, M. Schulz, S. Serrar, A. J. Simmons, M. Sofiev, M. Suttie, A. M. Tompkins, A. Untch, Aerosol analysis and forecast in the european centre for medium-range weather forecasts integrated forecast system: Forward

modeling, Journal of Geophysical Research: Atmospheres 114 (D6) (2009). arXiv:https://agupubs.onlinelibrary.wiley.com/doi/pdf/10.1029/2008JD011235, doi:https://doi.org/10.1029/2008JD011235. URL https://agupubs.onlinelibrary.wiley.com/doi/abs/10.1029/2008JD011235

[53] A. Mortier, P. Goloub, T. Podvin, C. Deroo, A. Chaikovsky, N. Ajtai, L. Blarel, D. Tanre, Y. Derimian, Detection and characterization of volcanic ash plumes over Lille during the Eyjafjallajökull eruption, Atmospheric Chemistry & Physics 13 (7) (2013) 3705–3720. doi:10.5194/acp-13-3705-2013.

[54] S. A. Clough, M. W. Shephard, E. J. Mlawer, J. S. Delamere, M. J. Iacono, K. Cady-Pereira, S. Boukabara, P. D. Brown, Atmospheric radiative transfer modeling: a summary of the AER codes, Journal of Quantitative Spectroscopy and Radiative Transfer 91 (2) (2005) 233–244. doi:10.1016/j.jqsrt.2004.05.058.

[55] L. S. Rothman, I. E. Gordon, Y. Babikov, A. Barbe, D. Chris Benner, P. F. Bernath, M. Birk, L. Bizzocchi, V. Boudon, L. R. Brown, A. Campargue, K. Chance, E. A. Cohen, L. H. Coudert, V. M. Devi, B. J. Drouin, A. Fayt, J. M. Flaud, R. R. Gamache, J. J. Harrison, J. M. Hartmann, C. Hill, J. T. Hodges, D. Jacquemart, A. Jolly, J. Lamouroux, R. J. Le Roy, G. Li, D. A. Long, O. M. Lyulin, C. J. Mackie, S. T. Massie, S. Mikhailenko, H. S. P. Müller, O. V. Naumenko, A. V. Nikitin, J. Orphal, V. Perevalov, A. Perrin, E. R. Polovtseva, C. Richard, M. A. H. Smith, E. Starikova, K. Sung, S. Tashkun, J. Tennyson, G. C. Toon, V. G. Tyuterev, G. Wagner, The HITRAN2012 molecular spectroscopic database, Journal of Quantitative Spectroscopy and Radiative Transfer 130 (2013) 4–50. doi:10.1016/j.jqsrt.2013.07.002.

[56] ESA, Report for mission selection: Forum, Tech. Rep. ESA-EOPSM-FORM-RP-3549, 263pp., European Space Agency, Noordwijk, The Nether-

lands, https://esamultimedia.esa.int/docs/EarthObservation/EE9-FORUM-RfMS-ESA-v1.0-FINAL.pdf (accessed on 29 October 2020) (2019).

[57] Q. Fu, P. Yang, W. B. Sun, An Accurate Parameterization of the Infrared Radiative Properties of Cirrus Clouds for Climate Models., Journal of Climate 11 (9) (1998) 2223–2237. doi:10.1175/1520-0442(1998)011<2223:AAPOTI>2.0.CO;2.

[58] J. Ding, P. Yang, G. W. Kattawar, M. D. King, S. Platnick, K. G. Meyer, Validation of quasi-invariant ice cloud radiative quantities with MODIS satellite-based cloud property retrievals, Journal of Quantitative Spectroscopy and Radiative Transfer 194 (2017) 47–57. doi:10.1016/j.jqsrt.2017.03.025.

[59] D. T. Gillespie, The Monte Carlo Method of Evaluating Integrals, Naval Weapons Center, China Lake, CA, USA, 1975, https://apps.dtic.mil/dtic/tr/fulltext/u2/a005891.pdf.

[60] S. Platnick, P. Hubanks, K. Meyer, M. D. King, Modis atmosphere l3 monthly product, Tech. Rep. MODIS Collection 6.1 - Level 1, Atmosphere, Land (ArchiveSet 61), NASA MODIS Adaptive Processing System, Goddard Space Flight Center, USA, http://dx.doi.org/10.5067/MODIS/MYD08_M3.061 (accessed on 23 December 2020) (2015).

[61] P. Hubanks, S. Platnick, M. King, B. Ridgway, Modis atmosphere l3 gridded product algorithm theoretical basis document (atbd) and users guide (2019).